Addis Ababa University

Addis Ababa Institute of Technology

African Railway Centre of Excellence

Analysis of Crack Initiation and Fatigue Life on Light Rail Transit (LRT) Wheel Tread Profile: A Finite Element Approach.

A Research submitted to the school of Graduate Studies of Addis Ababa University in Partial Fulfilment of the Requirements for the Degree of Master of Science in Railway Engineering (Rolling Stock)

BY:

Kaggwa William Namutale

Thesis Advisor: *Dr. Araya Abera Betelie*

May, 2025

Addis Ababa, Ethiopia

Declaration

I declare that the work presented in this thesis document titled "Analysis of crack initiation and fatigue life on Light Rail Transit (LRT) wheel tread profile: A finite element approach" is my own independent research work and has not been submitted for any academic award at any other university or institution. I also confirm that all referenced material and received assistance have been properly cited, acknowledged, and duly credited.

Name: ***Kaggwa William Namutale***

Signature: …….. Date: …….

Advisor: ***Dr. Araya Abera Betelie***

Signature: …….. Date: …….

Approval

A thesis submitted to African Railway Centre of Excellence, Addis Ababa Institute of Technology, and School of Graduate Studies in partial fulfilment of the requirement of the award of Degree of Masters of Science in Railway Engineering (Rolling Stock)

Submitted by:

Kaggwa William Namutale	_____	_____
Student	Signature	Date

Approved by:

Dr. Araya Abera Betelie	_____	_____
Advisor	Signature	Date

Examiners

Dr. Habtamu Tkubet	_____	_____
Examiner 1	Signature	Date
Mr. Biniyam Ayalew	_____	_____
Examiner 2	Signature	Date

Acknowledgement

Great thanks to the God Almighty for giving me the patience and strength through this learning phase of research.

Great appreciation to *Dr. Araya Abera Betelie* and all examiners for their understanding, friendship, guidance, and patience throughout this research. Their mentorship and guidance has played a key role in the smooth completion of this study work. Working under your guidance and expertize is an exceptional privilege and honor.

To my family, thank you for all the support and understanding given through this life phase; may God continue blessing you!

To the African Railway Center of Excellence at Addis Ababa University and World Bank, am thankful for the opportunity given and the facilitation offered to attain this level of training and education.

Abstract

The conditions within which railroad wheels operate, damage to their treads is inevitable. The damage ranges between minor (scratches) to major (fatigue cracks). This has advocated for studies and investigations into the various parameters that lead to their damage; included among the parameters is crack initiation (formation), propagation, and fatigue. This study, aimed at not only looking into the parameters that influence crack initiation but also dwell into investigations into the effects of varying the loading conditions and crack orientation on the stress distributions at the wheel tread surface and thereafter the effects of varying the crack lengths in the region of maximum stress concentration to the fatigue life cycles (cycles per mm growth). The research employs a model developed in SOLIDWORKS modelling software, and analyzed using both ANSYS and FRANC3D tools. Results showed that maximum stress occurs when cracks are aligned in the direction of motion, exceeding the material's ultimate tensile strength at overload capacity. Fatigue life analysis further revealed a strong dependency of the cycles on crack length. The study underscores the role of stress intensity factors and crack length in predicting fatigue life cycles.

Keywords: Crack Initiation, Crack Orientation, Stress Distribution, Fatigue Life, Railroad Wheel Tread surface, Finite Element Approach.

List of Abbreviations and Acronyms

Term	Explanation / Meaning
APDL	ANSYS Parametric Design Language
CYS	Compressive Yield Strength
DOF	Degree of Freedom
FE-	Finite Element -
FEA	Finite Element Analysis
FRANC3D	Fracture Analysis Code 3-Dimensional
J-S	Jiang-Sehitoglu
LCF	Low Cycle Fatigue
LEFM	Linear Elastic Fracture Mechanics
LRT	Light Rail Transit
MBS	Multi-Body System
MSS	Maximum Shear Stress
MTS	Maximum Tensile Stress
Ne	Fatigue Life Cycles
RCF	Rolling Contact Fatigue
SIF	Stress Intensity Factor
SWT	Smith Watson Topper
UTS	Ultimate Tensile Strength
W_o	Overload Weight
W_R	Rated Weight

Table of Contents

List of Figures

List of Tables

Chapter 1: Introduction

1.1 Background

All over the world, railway transport has made its name in movement of passengers and/with their goods on interconnected tracks. The tracks network have grown in number due to increase interconnectivity projects all around the world. The continuous and increased use of this transport mode is majorly because of its safety, reliability, efficiency, and its capability to move long distances with enormous loads (cargo or passengers) especially in places where it is well developed and implemented [1]. The safety of the system greatly relies on risk assessment, dynamic quality modelling, improved technologies including robotics and artificial intelligence, and traffic assessment among others. Managing all identified risk points is important in all operations to avoid catastrophes occurring. With highly optimized systems such as robots and Artificial Intelligence (AI), predicting and managing these risks gets easier each passing day [2].

Not only is the safety crucial with just passengers, however, with hazardous goods too as they pose equal or worse dangers to both people and the environment. Railway transport operations' safety is influenced by several key factors including; infrastructure which comprises the condition of tracks, bridges, signals, and tunnels; followed by the rolling stock's design, maintenance, and working condition over time; human factors circling around the actions of train operators, maintenance personnel, and other staff; weather conditions, such as heavy rain, snow, or fog [3].

Focusing particularly on rolling stock safety, component designs and locomotives are rigorously checked by engineers together with safety experts using reviews, simulations, testing (prototypes and physically), and certification, for structural integrity and crashworthiness [4]. All these are done to assess, verify, and validate the strength, durability, endurance, and performance of all components and features under various conditions expected during their operation. To operate in any country, regulatory authorities and governing bodies always give compliance standards for which all rolling stock must fulfill for implementation. The checks are continuously done even after installation through periodic inspections, performance monitoring, and regular or scheduled maintenance [5]. A review by Pradeep et al. shows that most of the railway accidents are caused

by rolling stock failures (Figure 1) with the axle and wheel accounting for 41% and 19% respectively of the valued accidents [6].

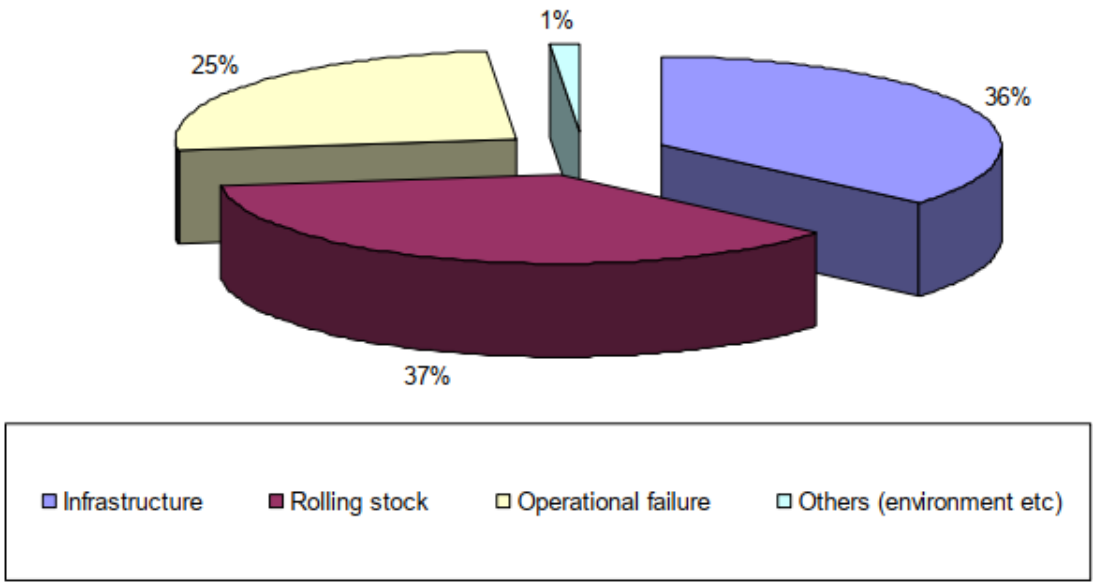

Figure 1: *Causes of railway accidents (data from across 23 countries)[6].*

Among the critical components is the wheel, whose failure brings significant implications to the safety and operational efficiency for the entire railway network. However much failures of its sort are rare, they render catastrophic derailments. This has prompted extensive research into the mechanisms and failure modes essentially to develop strategies that can effectively mitigate risks associated with failures of the wheel components [7], [8].

Figure 2: *Cracking on the wheel tread [7].*

Wheel surface damage (Figure 2) is among the most problematic issues in the railway industry [9]. In assessing and validating the components structural integrity, various techniques such as mathematical computation, Finite Element Analysis (FEA), Dynamic analysis, material modelling, Fatigue analysis, and crashworthiness simulations are used. Based on the tremendous reduction in the running costs, the FEA has gained popularity with the advancement in software technology and fast data processing computers [10].

Current studies have shown substantial progress on crack initiation, propagation, and fatigue life of railroad wheels. Most studies have neglected the effects of temperature, varying wheel loads, and speeds [11] which are very important for predictions related to the real-world conditions. While work has been done using material and stress models in FEA, the material properties are much simplified, the coupled thermal-mechanical stress models and dynamic load effects are underexplored [12], [13], which reduces the accuracy of the simulations. Furthermore, some studies have focused on specific conditions (such as partial slip models, High-Cycle Fatigue (HCF)) and therefore lack scenarios with varying wheel geometries and materials and Low-cycle fatigue [14].

With the software-based FEA's popularity, it hasn't been fully employed to investigate and analyze crack initiation in wheels and rails for the railway sector. Available papers indicate that only limited amount of research has been conducted using the approach. Most studies that were accessed used experimental and numerical approaches on wheels and rails for heavy haul trains [15], [16].

In a positive light, the studies show collective efforts dedicated to understanding crack initiation and fatigue life in railroad wheels and a strong motivation to further improve the network. Significant advancements employ innovative methods and software such as XFEM, Multiaxial stress analysis, and thermal-mechanical loading. Nonetheless, comprehensive models capturing most operational and environmental factors, stress interactions, and material properties, have hindered the applicability of most findings in the real-time conditions of the railway transportation sector.

Therefore, this study intends to serve as an additional building stone to these works by employing the Finite Element Approach to analyze crack initiation and fatigue life on LRT wheel treads for

which the results could be used in developing and/or improving of preventive maintenance strategies.

1.2 Statement of the Problem

The wheel is one of the most critical components in a railway system and holds all the forces exerted by the whole rolling stock and transmits it to the rail. Light Rail Transit (LRT) systems, such as the Addis Ababa LRT, operate under urban conditions of frequent acceleration and braking, straight and tight curves, and high passenger turnover that induce localized stress concentrations and cyclic loading patterns markedly different from those in heavy-haul or main-line rail. Failure of the wheel during operation could lead to fatalities, damage to assets, and operation disruptions; hence losses to the entire LRT service [17], [18], [19].

With most work focused on wheel tread substructures and heavy-duty systems, the mismatch creates a knowledge gap: without LRT-specific stress analyses, crack-growth predictions, and life-cycle estimates, urban rail operators risk undetected surface damage, unexpected wheel failures, and costly service interruptions. To address some of these, this study focuses on developing an FE-approach workflow for exclusively LRT wheel tread surfaces on a straight track.

1.3 Research Questions

This research aims at answering the following questions:

1. How does varying the loading conditions affect the distribution of stresses at the wheel tread?
2. How can fatigue life at a cracked wheel tread surface be predicted?
3. What is the effect of varying crack lengths using specified loading conditions on the overall fatigue life?

1.4 Objectives

1.4.1 General Objective

The general objective of the research is to analyze the crack initiation at LRT wheel treads and determine the corresponding fatigue life by considering the FE approach.

1.4.2 Specific Objectives

- To determine the effect of varying loading conditions on the stress distributions on the wheel tread surface.
- To assess the influence of different crack orientations on the magnitude and location of stress concentration on the wheel tread surface.
- To predict the fatigue life for cracked wheel tread surface.
- To investigate the effect of varying the crack lengths using specified loading conditions on overall fatigue life of the wheel.

1.5 Significance

Wheel failure remains a significant safety challenge in the railway sector. Understanding the factors that contribute to this failure has led to improved designs and optimized material selection. By gaining a deeper comprehension of parameters such as crack initiation and fatigue life, there is potential to enhance safety, durability, and reliability of wheels during railway operations.

This study aims to utilize available advanced computational methods to predict wheel tread failure, offering insights and methodologies that will aid in the optimization of the available mitigation strategies for preventive maintenance of railroad wheels.

1.6 Delimitations

In most recent developments, high-strength steel, exotic materials, and highly optimized but less common materials are increasingly used for wheel treads and wheels. However, this study will focus solely on materials commonly used as outlined in international standard manuals. While wheel treads experience extreme and rare conditions during operation, this analysis will be confined to nominal operating conditions. To address the complexity of wheel profile geometry, geometric simplifications will be applied to capture essential information with minimal omissions. Only commercially available FEA software will be employed. Finally, the validation of results will be restricted to published literature with established standard testing methods.

Chapter 2: Literature Review

The performance, safety, and reliability of Light Rail Transit (LRT) systems are largely determined by the behavior of the wheel/rail contact interface. This interface plays a critical role in the initiation of cracks and subsequent fatigue life of wheel treads, influencing the overall maintenance costs and operational downtime of the transit system. This literature review aims to critically assess the current state of knowledge regarding;

- The wheel/Rail contact interface
- The crack initiation at railroad wheel treads
- The factors influencing crack initiation of the treads
- The mechanisms leading to cracks being formed on wheel treads
- The available approaches for fatigue life analysis of the wheel treads
- FRacture ANalysis Code 3D (FRANC3D) software

Ultimately, identified key research gaps that will justify further study into LRT wheel tread analysis are provided after the *summary* at the end of this review.

2.1 The Wheel/Rail Contact Interface

The wheel/rail contact interface (Figure 3) is a critical aspect of railway vehicle dynamics and performance as it not only influences the mechanical behavior of trains but also their safety and efficiency. The complexities involved when understood allow optimization of the components and their operation hence reduction in their damage (wear). The interface majorly involves three types of forces: vertical (load-bearing), lateral (guiding), and longitudinal (traction). Each of these forces plays a vital role in the stability and performance of railway vehicles. The vertical force is responsible for supporting the weight of the train, while lateral forces help maintain alignment on the track, and longitudinal forces are crucial for acceleration and braking. The geometry of the wheel and rail significantly affect how these forces are distributed across the contact area [20].

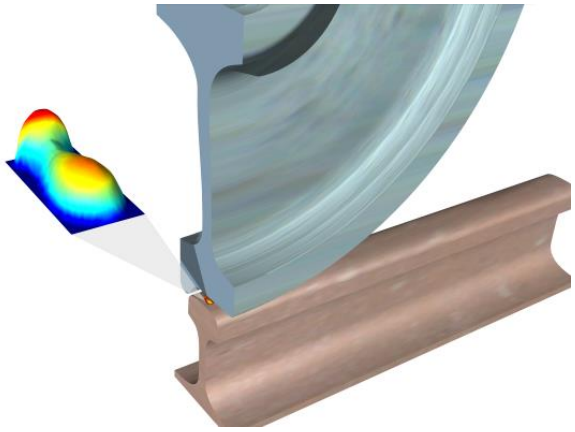

Figure 3: *Wheel/rail contact patch and qualitative surface plot (normal stress distribution) [20].*

The contact area between wheel and rail is typically small, often measuring 1 to 2 cm^2, yet it must support vertical loads that can exceed 10 tons. This results in high contact pressures, which can lead to material deformation. The contact patch is generally considered as a single point; however, under specific conditions, such as sharp curves or switch crossings, multiple contact points may occur [21]. Existing research, such as that by Lewis and Olofsson [22], outlines how contact forces lead to wear and rolling contact fatigue (RCF) in railway wheels.

In LRT systems, these forces manifest differently due to the lower axle loads and unique operational patterns. Most studies, however, have focused on heavy-duty rail systems, and the behavior of the wheel/rail interface in LRT systems remains relatively unexplored. This gap underlines the need for more specific studies on the dynamics of LRT systems.

2.2 Crack initiation at Railroad Wheel Treads

At the wheel-rail contact system (Figure 4), environmental factors like humidity, water, temperature, and external elements such as leaves have a significant impact due to the system's open nature [23].

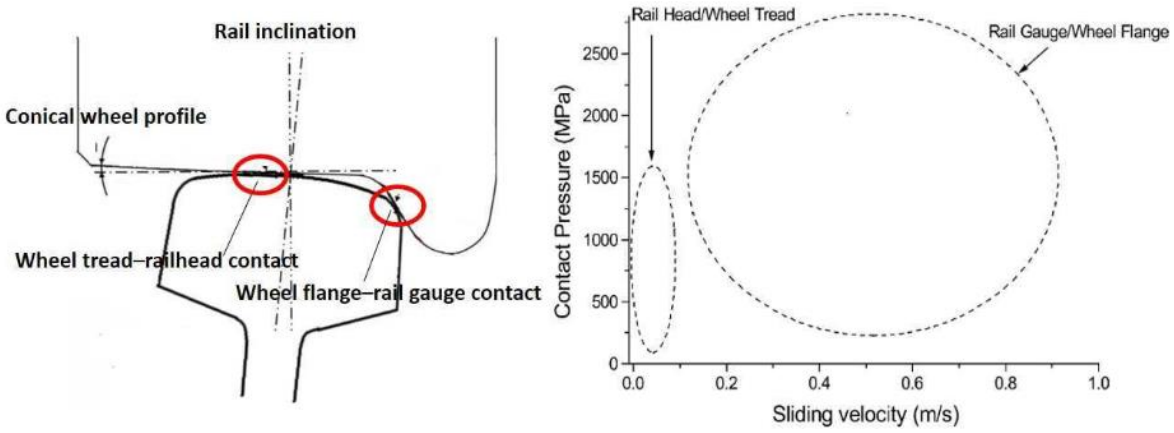

Figure 4: *Wheel rail contact system [23]*

For the wheel tread, significant factors contributing to formation of a crack (crack initiation) include temperature variations [24], [25], wheel out-of-roundness [26], spalling [27], rolling contact fatigue (RCF) [16], [27], shelling, thermal cracking, and wear [28], [29]. Current research on crack formation at the tread is dedicated to the initiation parameters, microstructural changes, and developing predictive models [30], [31], [32], all of which are influenced by the aforementioned factors affecting wheel treads.

2.3 The Factors leading to crack formation

The factors highlighted below explain the complex relation (external and internal) between material properties, mechanical stresses, and operational conditions in the initiation of cracks in train wheels.

- Rolling Contact Fatigue (RCF): Repeated stresses at the wheel-rail contact can lead to RCF hence high stresses at the surfaces of the wheel [27].
- Static Stress and Material Fatigue: Cracking can be caused by failure to comply with the necessary loading requirements, leading to increased static stress, or by material fatigue due to dynamic conditions [33].
- Internal Defects: Cracks can initiate from internal defects such as nonmetallic inclusions or voids, particularly in heavy haul freight car wheels. Larger defects tend to lead to faster crack propagation [34].

- Increased wheel-rail interaction forces: Increase in wheel–rail interaction force influences the initiation of cracks. This may be due to changes in the operation speed of the train, wheel diameters, and the resonant frequencies of the wheels [35].
- Axle Load and Friction Coefficient: Higher axle loads increase the maximum contact normal stress, Von Mises stress, and increase in the static friction between the wheel and rail. These factors are also known to affect RCF crack initiation [36].

These factors promote and increase the likelihood of cracks forming through offering a conducive environment that induces stress needed for crack formation over a period of time.

2.4 Mechanisms of Crack Initiation in Railroad Wheel Treads

The mechanisms explain how cracks start forming at microscopic level as a result of the above mentioned factors. These mechanisms include cyclic loadings (RCF and LCF) and thermal loading fatigue, corrosion-assisted cracks (from chemical reactions), creep (from constant stress), and stress concentrations (especially at manufacturing flaws) [37].

Majorly related to the research topic (crack initiation at wheel treads) is RCF and LCF hence further discussed.

2.4.1 Rolling Contact Fatigue (RCF)

Rolling contact fatigue is a primary failure mode in railway wheel treads. RCF occurs due to repeated loading and unloading cycles, leading to the formation of micro-cracks. Key factors influencing RCF include:

- Contact Stress: High contact stresses at the wheel-rail interface result from wheel loads and dynamic forces.
- Material Properties: The mechanical properties of wheel materials, such as hardness and toughness, significantly impact crack initiation.
- Environmental Conditions: Factors like temperature, humidity, and presence of contaminants can affect wear and fatigue life

2.4.2 Low-Cycle Fatigue (LCF)

Low-cycle fatigue is characterized by the accumulation of plastic deformation during cyclic loading. In the context of LRT, LCF is particularly relevant due to frequent stops and starts, which impose significant stress on wheel components.

- Plastic Strain Accumulation: As plastic strains accumulate, they can lead to crack initiation, especially in regions subjected to high stress concentrations.
- Ratcheting: This phenomenon occurs when cyclic loading leads to progressive plastic deformation, further contributing to crack development.

The analysis of the factors and mechanisms for crack initiation at wheel treads follows several approaches as reviewed in the next section.

2.5 Approaches for Crack Initiation Analysis for Railroad Wheel Treads

Approaches for analysis of crack initiation are tools and methods used to predict and mitigate crack initiation at wheel treads. These approaches can generally be grouped into three (3) that is Experimental, Numerical, and Simulation or Finite Element approaches.

2.5.1 Experimental Approaches

Zhu [23] categories these into three common approaches which are small-scale scaled test-rigs, and full-scale experimental approaches as shown in **Figure 5** below. Table 1 summarizes the advantages and disadvantages of each experimental approach.

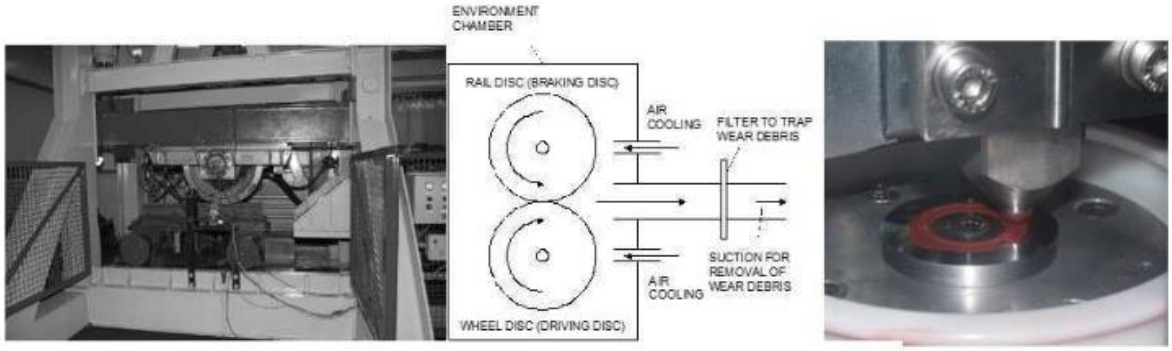

Figure 5: *Full-Scale (Left), Twin-Disc (Middle), and Pin-on-Disc (Right) Laboratory-based testing methods [23].*

Table 1: *Advantages and disadvantages of experimental approaches*

Test Approach	Advantages	Disadvantages
Pin-on-disc	Quick and cheap to run; specimens can be cut from actual wheel and rail; good control over test parameters; easy to take measurements; easy to add 3rd body materials; environmental chambers can be added	Full-sliding (can assess limited scenarios such as sharp curves, although can be considered to simulate the "slip" part of a partially sliding contact); simplified contact geometry
Twin-disc	Easy to run; specimens can be cut from actual wheel and rail good control over test parameters; easy to take measurements; easy to add 3rd body materials	Simplified contact geometry; Hard to achieve environmental conditions
Scaled wheel-rail	Contact conditions more representative	Specimens expensive and hard to procure; measurements harder to take accurately
Full-scale laboratory	Actual contact conditions; actual components usually	Tests expensive and time consuming; control over test conditions more limited; measurements hard to take accurately
Field	Actual environmental and contact conditions	No control over contact conditions; hard to obtain data; no friction data

A review by Zhang [37] properly explained the numerical and the FE-Approaches. The details of each are summarized in the proceeding sections.

2.5.2 Numerical Simulation/Mathematical Approaches

- The shakedown map: An experimental method which gives the regions (ratcheting, plastic deformation, elastic or elastic deformation) for calculation of crack initiation life. However, it uses a range of data instead of precise data. Therefore, need for future study to

determine whether the points on the existing shakedown limits are accurate or not in railway operations.

- Cyclic Constitutive models: These include Chaboche model (combines isotropic and non-linear kinematic hardening law) in which the yield surface is free to move in stress space and change shape or size but the model can't synchronously simulate the non-linear behavior or ratcheting rate and also over-predicts the biaxial and multiaxial ratcheting responses; J-S model (uses non-linear kinematic law) which gives the best representation of shape and width of the stress-strain curve, the ratcheting rate, and better cyclic response, with a complex formulation though; and the Bower model (also uses the non-linear kinematic law) which gives a more stable numerical behavior for high-load levels due to a less complex formulation than J-S but with an unreliable physical cyclic response compared to that of J-S.
- Crack initiation criterion: This applies the JS-SWT/CXH criterion combination to obtain the normal and shear components of stress and strain together with the stress amplitude.
- Critical plane which employs observation of the crack initiation and propagation to obtain the maximum fatigue parameter. However, the method misses critical planes for wheels.

2.5.3 Simulation/FE- Approaches

These can be broadly categorized into Finite Element Analysis (FEA) and dynamic simulation (Multi-body system, MBS) about wheel-rail modelling.

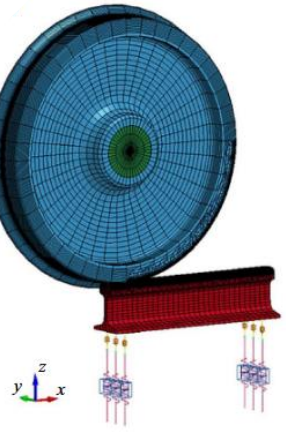

Figure 6:*3D FEA model [37].*

These are mostly used since field dynamic characteristics are difficult to determine. They can be subdivided into the following:

- 2D and 3D FEA: These are limited by absence of many contact parameters (for 2D) and field dynamic parameters (for 3D).
- MBS: Highly effective however complex and requires long computation time.

2.5.4 Monitoring Approaches

These have been developed to detect and assess cracks on wheel treads. Broadly, they are categorized into two; that is, direct and indirect monitoring techniques [17], [19], as explained below.

- Direct Monitoring Techniques

These use sensory equipment to detect abnormalities such as cracks directly on the wheel surfaces the tread included. They employ methods such as visual and ultrasonic inspections, acoustic emission sensors that detect high-frequency waves as emitted by rapid energy released from cracks, and infrared thermography which monitors the thermal patterns (heat distribution) on the wheel surfaces. While the acoustic emission sensors and infrared thermography can offer real-time data, the visual and ultrasonic face the biggest drawback of the need for removal of wheels from service for inspection, making the process time consuming.

- Indirect Monitoring Techniques

These techniques are employed to monitor parameters that indicate the presence of cracks in wheels. Parameters such as vibrations, impact forces, and acoustic signals are monitored. Through vibration analyses, vibration signatures registered have changes that infer presence of cracks within the component. Wheel Impact Load Detectors (WILD) measure the impact forces generated by wheels as they pass over the sensors mounted on the track; anomalies in the measured values indicate cracks or flats on the surfaces of the wheel. Accelerometers positioned near the track register signals from the interaction of the wheel and rail.

These techniques are usually integrated such as acoustic emission sensors with infrared thermography to obtain comprehensive data on the cracks and their location. The effectiveness of any technique as employed is affected by factors such as the environment, analysis technology, and sensory technology.

2.6 Fracture Analysis Code 3D (FRANC3D)

2.6.1 Introduction

Pre-existing crack will be introduced in the model using FRANC3D to incorporate a range of crack lengths chosen from available literature. The material properties, loading and boundary conditions will be as those implemented in the CAD model analysis performed earlier and a comprehensive analysis will be carried out. FRANC3D will be utilized for fatigue calculations (integrating ANSYS capabilities in the FE-Software) using stress and strain data together with crack length calculations to determine fatigue life and other damage parameters for the cracked wheel tread.

2.6.2 Overview of FRANC3D/NG

The *FRacture ANalysis Code 3D/Next Generation* (FRANC3D/NG) is a specialized software designed to simulate the progression of cracks in complex engineering structures. By integrating seamlessly with finite element analysis (FEA) programs like ANSYS, ABAQUS, and NASTRAN, FRANC3D/NG expands their functionality to handle intricate crack modeling tasks. The software's focus lies in addressing situations where the structural configuration, applied loads, and evolving crack shapes are highly complex as is the case for the wheel/rail contact interface. Updated versions of the software allow analysts to study the behavior of cracks more precisely especially for critical geometries and loading states [38].

2.6.3 Integration with FEA Tools and Workflows

FRANC3D/NG communicates with FEA platforms through mesh files, adhering to widely accepted formats like `.cdb` (ANSYS), `.inp` (ABAQUS), and `.bnf` (NASTRAN). This interoperability allows the user to:

1. Develop base models without cracks in their preferred FEA software.
2. Import these models into FRANC3D/NG to simulate crack evolution.

3. Export the updated mesh back to the original FEA tool for further processing.

The software adopts a localized analysis approach (**Figure 7**), focusing computational resources on sub-models that represent the crack regions. This ensures efficient processing without compromising the overall accuracy of the simulation. The built model(s) in ANSYS environment are exported to FRANC3D in form of ".cdb" where the cracks are inserted, remeshed, and then analyzed using the ANSYS executable. The approach merges the capabilities of both analysis software (in this case, ANSYS and FRANC3D) to predict the damage that the cracks can impose.

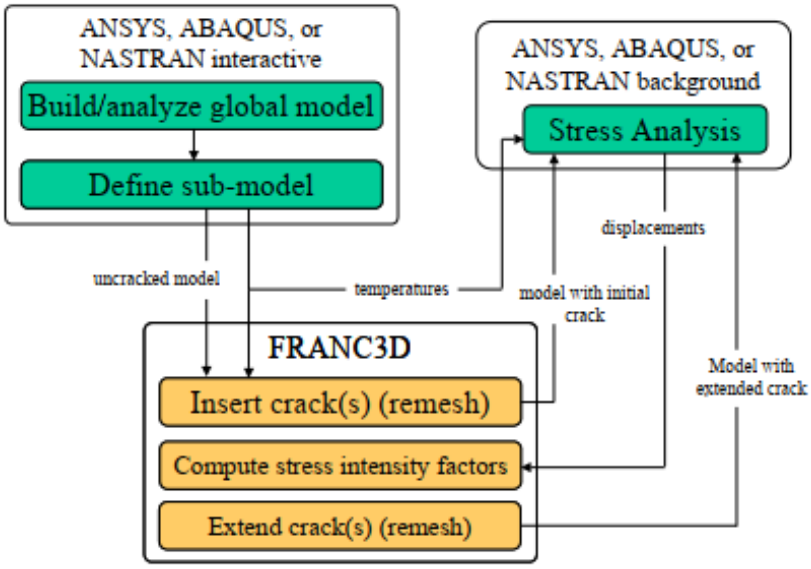

Figure 7: *Workflow in FRANC3D [38]*

2.6.4 Key Features of Crack Analysis

The crack analysis involves initial setup of the model using tools such as ANSYS-APDL, isolating a specific are for detailed crack-related simulations, use of numerical criteria (such as J-integrals and Maximum Tensile Stress) within the software to evaluate SIFs, mesh refinement, integration, and reanalyzing the modified model for further evaluation.

This cycle allows FRANC3D/NG to handle mixed-mode loadings and simulate realistic, 3D crack trajectories.

2.6.5 Theoretical Basis for Damage Modeling

FRANC3D/NG leverages well-established principles of fracture mechanics to model damage progression, namely:

1. Stress Intensity Factors (SIFs): These parameters are used to understand how cracks advance under different loading modes.
2. Fatigue Crack Growth Laws: The software implements models like the Paris Law and the NASGRO equation to simulate fatigue-induced crack propagation.
3. Energy Release Metrics: Techniques such as the J-integral and M-integral assess energy changes at the crack front, aiding in the calculation of crack growth rates.

These capabilities ensure the software provides robust and scientifically grounded results for crack simulations hence its use in the current research.

2.6.6 Damage Equations and Principles Relevant To FRANC3D

As mentioned above, the principles and damage equations related to FRANC3D are described in this section.

- *The Stress Intensity Factors (SIF):*

  The SIFs characterize the stress state at the crack tip for the three modes of loading that is;

  - Mode I (K_I): Opening mode (tensile stress perpendicular to the crack).
  - Mode II (K_{II}): Sliding mode (shear stress in-plane with the crack).
  - Mode III (K_{III}): Tearing mode (shear stress out-of-plane)

  The general equation *i below* is used for the evaluation

$$SIF, K = \sigma\sqrt{\pi a} \cdot f \qquad \ldots \boldsymbol{i}$$

  Where $\sigma - Applied\ stress$

  $a - crack\ length$

  $f - Geometry\ correction\ factor$

- *The Paris' law*

  The law relates the crack growth rate to the range of the Mode I (ΔK) loading using equation *(ii)*

$$Crack\ growth\ rate, \frac{da}{dN} = C(\Delta K)^m \quad \textbf{...ii}$$

  Where $\Delta K = K_{max} - K_{min}$

  $C, m - Material\ constants$

  Within the software, the equation can be extended for mixed-mode loading by including the effects of K_{II} and K_{III}.

- *NASGRO Equation*

  The equation *(iii)* below known as the *NASGRO* equation refines Paris' law to account for threshold effects, material crack closure, and eventual fracture (fatigue life).

$$\frac{da}{dN} = C\left(\frac{\Delta K - \Delta K_{th}}{1-R}\right) \cdot \left(1 - \frac{K_{max}}{K_c}\right)^p \quad \textbf{...iii}$$

  Where $R, stress\ ratio = \frac{K_{max}}{K_{min}}$

  $p, m - material\ constants$

  $\Delta K_{th} - Threshold\ SIF\ below\ which\ no\ crack\ growth\ occurs$

  $K_c - critical\ SIF\ for\ fracture$

- *J-integral (energy release rate)*

  In the software, this is used for Linear Elastic Fracture Mechanics (LEFM). It calculates the total strain energy release rate for a crack under elastic-plastic or linear-elastic conditions using equation (*iv*) below.

$$J = \int_{\Gamma} \left(W\delta_{ij} - \sigma_{ij} \frac{\partial u_i}{\partial x_1} \right) n_j d\Gamma \qquad \textbf{...iv}$$

Where $W - strain\ energy\ density$

$\sigma_{ij} - strain\ tensor\ components$

$\frac{\partial u_i}{\partial x_1} - strain\ gradient$

$n_j - \Gamma' s\ normal\ vector$

- *Maximum Tensile Stress (MTS) criterion*

  The criterion (equation *v*) predicts the direction of crack growth under mixed-mode loading.

$$\theta_c = \frac{1}{2} \tan^{-1} \left(\frac{3K_{II}}{K_I} \right) \qquad \textbf{...v}$$

Where $\theta_c -$ Angle of crack growth

Crack Growth Increment

This follows relative crack growth for each step based on the SIFs and a crack growth law (e.g., Paris or NASGRO). The equation (*vi*) typically is

$$\Delta a = C(K_{eff})^m \cdot \Delta N \qquad \textbf{...vi}$$

Where $\Delta N - Number\ of\ cycles\ in\ the\ step$

$K_{eff} - Effective\ SIF$

- *Mixed mode effects*

  This is used by the software to compute for the equivalent SIF when the crack is subjected to combined loads. It uses equation (*vii*) below

$$K_{eq} = \sqrt{{K_I}^2 + \eta {K_{II}}^2 + \zeta {K_{III}}^2} \qquad \textbf{...vii}$$

Where $\eta, \zeta -$ Weighting factors for mode I and II depending on the loading conditions and material

2.6.7 Evaluation of Strengths and Limitations

FRANC3D/NG has demonstrated exceptional capability in modeling 3D crack propagation within a flexible framework using its modular design that supports integration with leading FEA tools, enabling advanced structural analyses. The focus on sub-modeling streamlines computational demands while preserving accuracy in crack-specific regions. Nonetheless, approximations in *mesh-based geometry* can limit accuracy, particularly for highly irregular surfaces. Additionally, although the software's graphical user interface and scripting options are intuitive, it requires knowledge in fracture mechanics to apply it effectively.

2.7 Critical Review

Kiani et al [11] in their paper on analysis of fatigue for wheels employed a multiaxial strain-based approach that focused on predicting how fatigue cracks initiate in railway wheels under complex loading conditions. The approach to analyses fatigue life with an aim to improve safety by preventing wheel failures. The methods involved finite element analysis (FEA) with the Chaboche plasticity model, which considers both isotropic and kinematic hardening to simulate the material response under cyclic stress. The study used ABAQUS to model wheel-rail contact, applying loads of 162kN and 233kN to evaluate stress and fatigue behavior. A multiaxial critical-plane approach was employed to assess how cracks form beneath the wheel surface. Results indicated that subsurface cracks initiated at a depth of 3.7 mm, and high-stress zones were identified as critical areas for fatigue failure. The study's predictions matched experimental observations, showing accurate crack initiation points under real-world loads. However, limitations include simplified material properties, which may not fully represent real operational conditions. Additionally, environmental factors like temperature and wear were not considered, which could affect the accuracy of fatigue life predictions.

The work by Jaifu et al [39] that studied the fatigue crack initiation location of wheel and rail under rolling contact using finite element method. This paper investigated the initiation of fatigue cracks in wheels and rails under rolling contact, emphasizing the significance of maintenance for rail transit systems. It highlighted how contact stresses from wheel-rail interactions could lead to fatigue damage, which is a common issue in rail operations. To conduct the study, the researchers employed the Finite Element Method (FEM) to create three-dimensional models of the UIC60E1 wheel and BS100 rail profiles. They varied the rail inclination angles and the lateral position of the wheel to analyze how these factors influenced contact stresses and fatigue crack initiation. The Dang Van criterion was applied to assess the likelihood of crack formation based on the stress data obtained from the simulations. The results indicated that the maximum Dang Van stress ratio was found at depths of 2.45 mm and 5.65 mm beneath the wheel and rail surfaces, respectively, suggesting that these areas were particularly susceptible to crack initiation. The study revealed that fatigue cracks were more likely to develop on the field side of the rail, especially with increasing rail inclination. However, the paper acknowledged some limitations, such as the need for further validation of the FEM results with experimental data to enhance reliability. Additionally, it pointed out that the study did not explore the effects of varying wheel loads or speeds, which could also significantly impact fatigue crack initiation.

Jang et al [12] presented a sophisticated model aimed at predicting the lifespan of railway wheels by examining the initiation of rolling contact fatigue cracks and the influence of residual stresses. The researchers employed a combination of experimental data and numerical simulations, integrating real-world measurements of wheel stress and fatigue into their model. They validated the model against existing data to ensure its accuracy. The results demonstrated that the model could effectively predict the initiation of fatigue cracks under various conditions, revealing that residual stresses could reduce the lifespan of railway wheels by up to 30%. However, the study's reliance on existing data may limit its applicability to all scenarios, and the model's accuracy could benefit from more extensive real-world testing.

Natnael [13] in his work on crack propagation investigated the growth pattern of a crack as a result of skidding together with added effects of friction (frictional heat load) and static mechanical load by employing Extended Finite Element Method (XFEM) and found that the crack tip stress and

plastic strain increased with increase of the crack length; Nonetheless, he suggested that at least the wheel cracks be modeled under 'fully coupled mechanical and thermal stresses' in XFEM, model the propagation of the crack under dynamic conditions in XFEM.

Furthermore, Wirtu [14] does a thermal-mechanical analysis of the W/R rolling/sliding contact. The model considered a tread-top for wheel and rail respectively with partial slip that was used to estimate the temperature rise. Results obtained showed the promotion of crack propagation and material fatigue with plastic strain appearing on and under the wheel tread. Also, with the indefinite increase in sliding velocity, the temperature and traction coefficients increased to extreme values. Besides checking the results experimentally, the research further suggested that work be carried out on extending the solution using non-Hertzian contact cases; analysis of LCF, profile wear and change of Wheel Rail materials, and the analysis of the contact using a different material.

Additionally, an investigation by Aklilu [40] on RCF (contact pressure, surface and subsurface stresses) on the wheel using the critical plane model in finite element with emphasis was on the orientation of the crack in determining the fatigue life found that friction, vertical loading, and wheel diameter were critical in determining the wheel's fatigue life; surface crack initiation occurred with increase in the traction force (higher frictional coefficient) while subsurface crack formation at lower frictional coefficients; the author's technique proved to be time saving. However, besides the limitation to computational efficiency, suggestions into inclusion of the effect of the track curvature and gradient, flange contact, investigation of lateral and spin creepages, and the effect of the rail geometry on fatigue analysis for the wheel were made.

A comprehensive review of published academic papers to assess research trends in the major components for the railway network (wheel and rail) was conducted in this study. The visual summary (Figure 8 and Figure 9) showcases the balance of research efforts and a perspective on which component has received more attention and which require additional exploration.

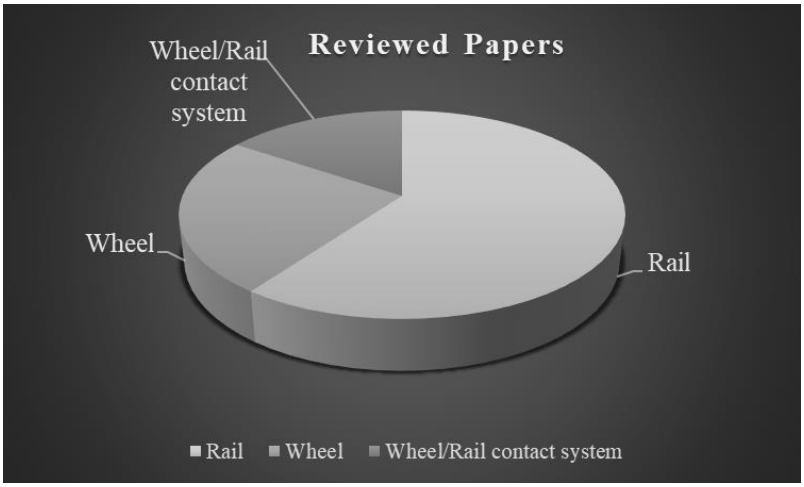

Figure 8: *Research paper distribution for rail, wheel, and wheel/rail contact system.*

Critical review of literature shows how the wheel/rail contact interface with all the imposed loads should certainly not fail. Research into crack initiation factors and mechanisms shows that RCF, LCF, axle loads, and coefficients of friction influence the formation of cracks at LRT wheel treads.

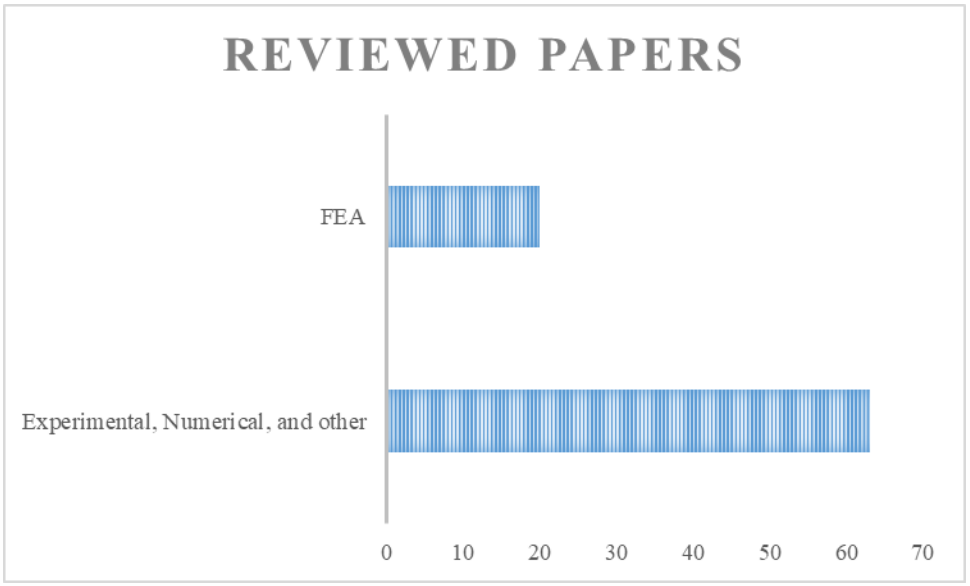

Figure 9: *Research approaches for the wheel reviewed papers*

Furthermore, the approaches for determining fatigue lives of cracked wheels comprising of the experimental, numerical, and simulation. Articles reveal critical planes and high pressure areas for crack initiation.

Table 2: *Literature review summary.*

Ref[]	Author(year)	Objective	Methodology	Findings
[39]	Aklilu (2022)	Investigate rolling contact fatigue and crack orientation.	- FEA-ABAQUS - Critical plane model - MATLAB	Increase in traction forces promoted crack initiation with subsurface cracks forming at lower coefficients of friction
[14]	Wirtu (2023)	Thermo-mechanical analysis of wheel-rail contact	- FEA-ANSYS - Hertz theory	Plastic strain on and under the wheel tread promoted crack propagation and material fatigue
[38]	Jaifu et al. (2018)	Location of fatigue initiated cracks of wheel and rail under rolling contact	- 3D-FEM - Dang Van damage criterion	Crack formation at 2.45mm below the wheel surface
[11]	Kiani et al. (2017)	Fatigue analysis of the railroad wheel	- 3D FEM - FEA-ABAQUS - Multiaxial strain-based critical plane index	Formation of cracks 3.7mm deep within the surface of wheel.
[13]	Natnael (2016)	Investigation of crack growth due to skidding	- FEA-ABAQUS - XFEM - Hertzian contact theory	Increase in stress and plastic strain at the crack tip with increase in the crack length

2.8 Research Gaps

While a considerable amount of research has focused on crack initiation and fatigue life analysis of the railroad wheel tread and heavy-duty railway systems, very little has been done for LRT systems, despite their distinct operational characteristics. The existing body of work tends to

overlook the lower axle loads, frequent stops, and different wheel geometries found in LRT. Additionally, most fatigue life models have been developed for freight rail applications and may not fully capture the dynamic loading conditions seen in LRT.

Key Gaps:

1. Limited research on LRT wheel treads as most existing models and experiments focus on substructure of the wheel and heavy-duty rail systems.
2. Limited predictive and simulation models tailored for LRT, that is, current simulations inadequately represent the real-world operational conditions of LRT.
3. Insufficient experimental data for LRT systems: The application of full-scale and twin-disc tests in LRT contexts remains unexplored.
4. Predictive model needed to help in decision making for maintenance scheduling and operations planning in with the state of the wheel.

Therefore, this research suggests a Finite Element Approach employing static analyses that integrates SolidWorks CAD modeling software capabilities, ANSYS software analysis tools, and FRANC3D fatigue and damage equations and theories embedded within the software, to determine fatigue life of a cracked railroad wheel treads under variable loading conditions. Great emphasis will be put on the effect of varying these loading conditions and chosen crack lengths to the tread and wheel entirely.

Chapter 3: Materials and Methods

In this section are the steps to be followed to obtain necessary results and validate them upon other related studies, some as discussed in the literature review, as related to the objectives of this research.

3.1 The Methodology Flow Chart

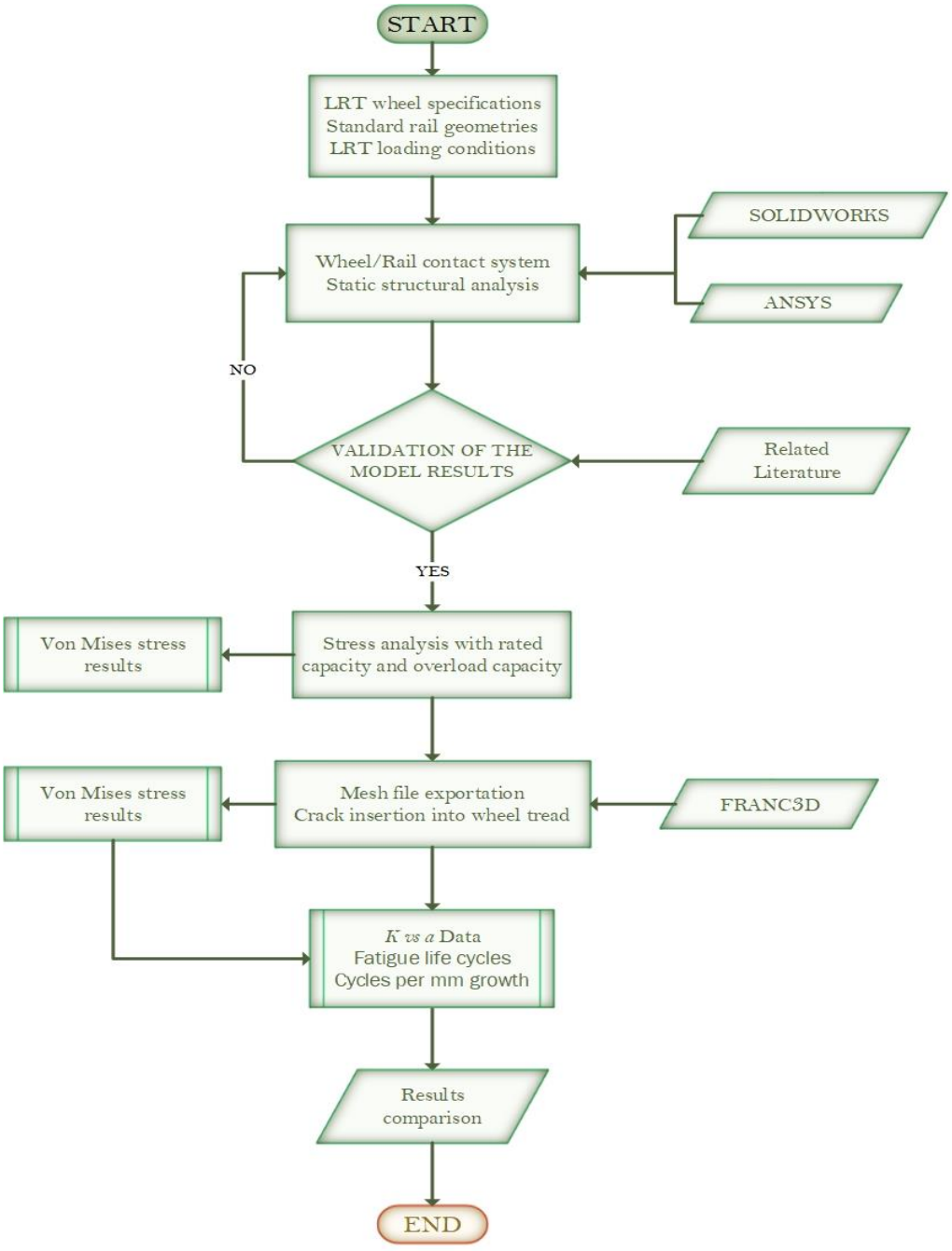

Figure 10: *Flow chart for the FE-Approach.*

3.2 Data Collection

Primary data gathered from Addis Ababa's sole Light Rail Transit service, encompasses material properties, wheel geometries, dimensions, and loading; while the secondary data includes research data obtained from legally published papers, journals, and international standards (such as EN and BS-EN).

3.2.1 Basic material parameters

The parameters are obtained from AALRT and standard manuals applying to new components. Figure 11 shows the nomenclature for the wheel (left) [41] and the rail (right) [42]. The wheel composition (Table 3) and mechanical properties for the wheel and rail are also provided in Table 4 as obtained from AALRT.

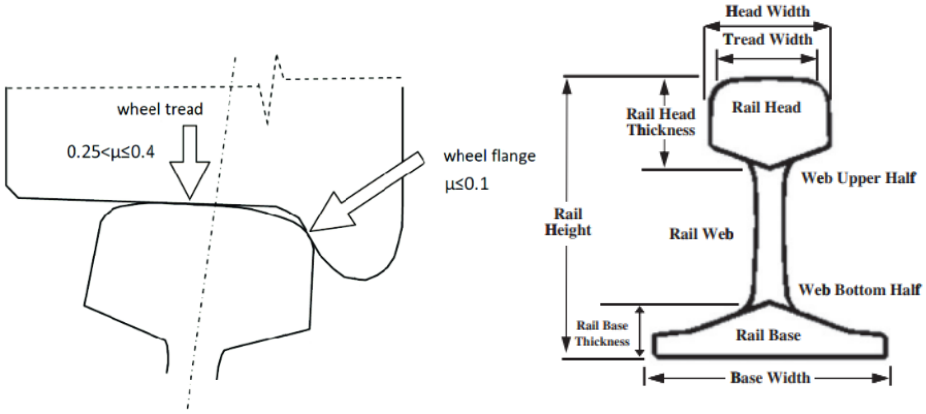

Figure 11: *Wheel (Left) and Rail (Right) Nomenclature*

Table 3: *Wheel chemical composition*

	Chemical composition (wt. %)					
	C	**Mn**	**Si**	**P**	**Ni**	**S**
Wheel	0.52	0.8	0.4	0.035	0.3	0.035

Table 4: *Wheel and rail mechanical properties (Reference: AALRT).*

	$E\ (GPa)$	v	$\rho\ (Kg/m^3)$	**UTS (MPa)**	**CYS (MPa)**	**Elongation (%)**

Wheel	210	0.3	7800	879	547	12
Rail	207	0.3	7800	880	640	12-15

3.2.2 Vehicle, Loading, and track condition.

AALRT vehicles are made up of three cars including a trailer car (Tp) positioned in between two motor cars (Mc1 and Mc2) as shown in Figure 12. The loading conditions and passenger data used for the two analyses, which is static analysis and fatigue analysis, are presented in Table 6 and Table 6. The data used is from AALRT design manuals considering 60kg as the average weight for each passenger. A straight-level track was considered for all analyses.

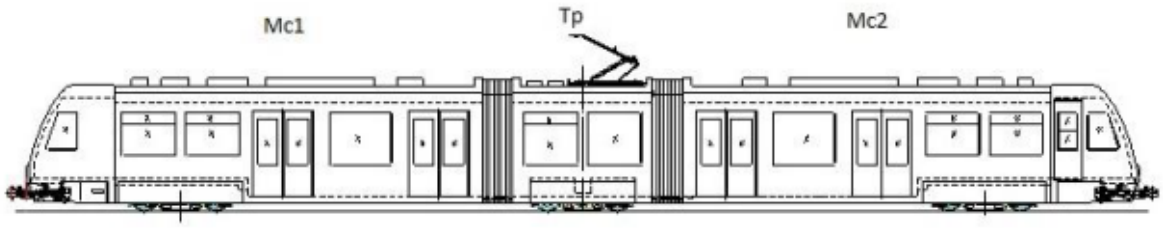

Figure 12: *AALRT vehicle (Source: AALRT)*

Table 5: *Passenger numbers as designed (Reference: AALRT)*

Number of passengers	Seated	Standing	Total
Level seats	65	0	65
Rated capacity (standing: 6 people/m2)	65	189	254
Overload capacity (standing: 8 People/m2)	65	252	317

Table 6: *Vehicle weight (Reference: AALRT)*

Loads	Car-body weight (t)	Passenger weight (t)	Total weight (t)	Axle Load (t)
Empty Vehicle	44	0	44	7

Seating capacity	44	15.24	59.24	10
Overload capacity	44	19.02	63.02	11

3.3 Geometrical Model

Using SolidWorks, a 3D model and sub-model (Figure 13) for the wheel and rail contact interface were created and saved in ".STEP" format for importing into ANSYS FE-software which will process the CAD file.

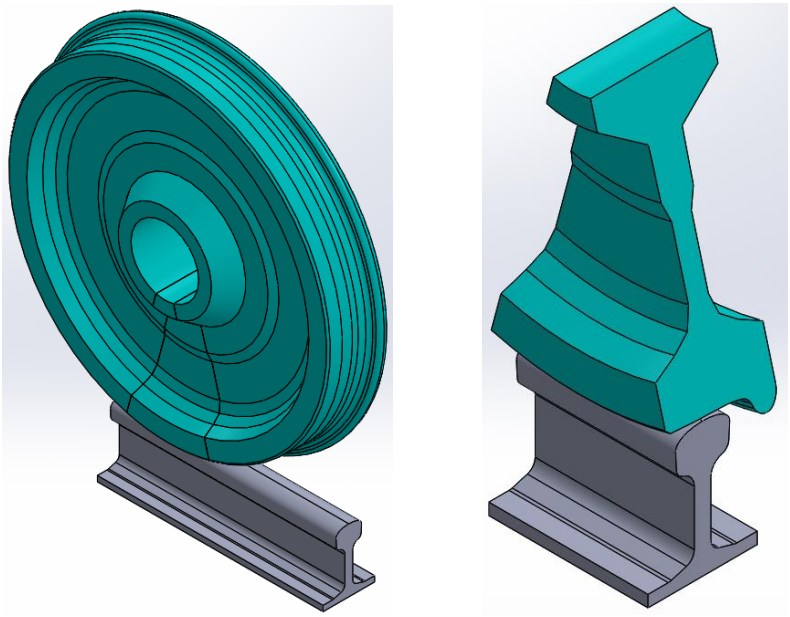

Figure 13: *3D model (Left) and Sub-model (Right) generated from SolidWorks*

3.5 FE – Model

The procedure in Figure 14 follows importing of the sub-model (.STEP file) into ANSYS Workbench platform.

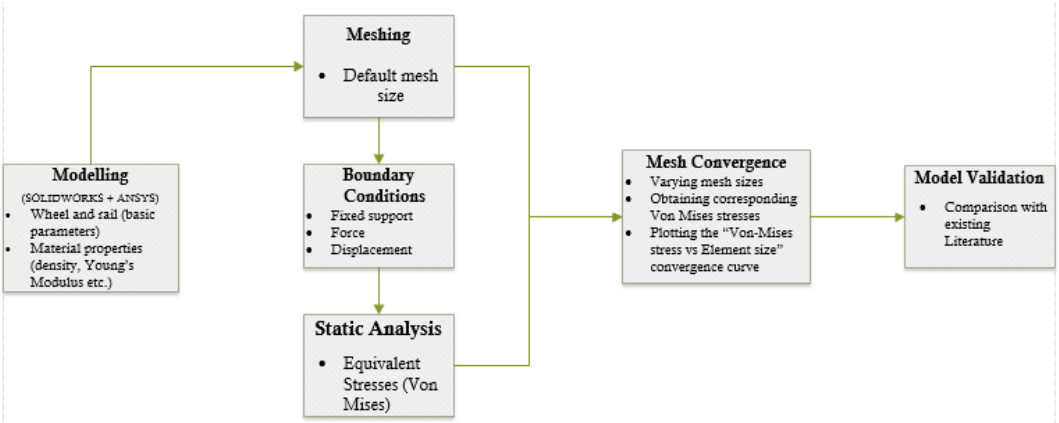

Figure 14: *The steps through Modeling to Validation.*

3.5.1 Sub-model Database Creation

This includes creating a *static analysis* database within the ANSYS Workbench and saving the *Project* with any desired name. Within this project, the imported model in Figure 15, can be accessed in the ANSYS Mechanical Enterprise, a component of the FE software package.

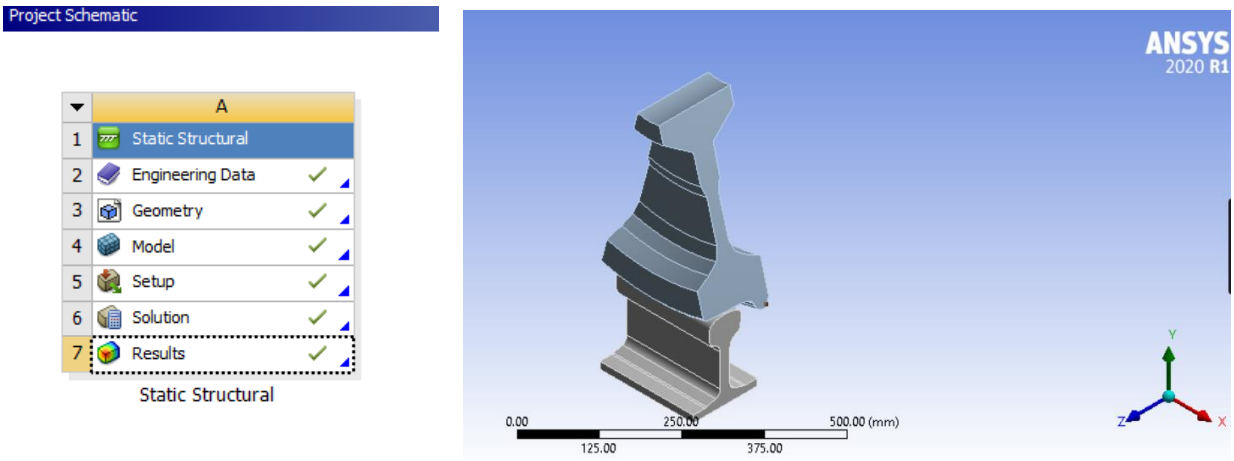

Figure 15*: The Project database (Left) and imported sub-model (Right)*

3.5.2 Analysis Steps (Pre- to Post-)

Assignment of the material properties (Table 4) for the wheel and rail is done and the contact condition for the selected model. Boundary conditions for the static analysis including fixed support, force, and displacement were then added as shown in Figure 16 below.

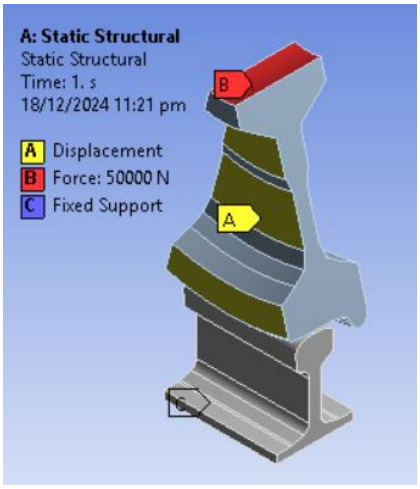

Figure 16: *The analysis' boundary conditions*

3.5.3 Solution

Using the *Structural* solver, the mathematical equations related to the *sub-model* are solved to get results for the problem (static analysis) as defined. Numerical approximations that use *Elements* are made within the software based on *Mesh* to compute the desired results (Von Mises stresses). The results are written in a Solution data file obtaining after the ANSYS monitor has ensured their convergence. The *Post-processor* allows visualization of the obtained results for interpretation [43].

3.5.4 Mesh Convergence

The convergence of the mesh ensures that the model being used for the simulations is valid enough with the results it gives. Finding convergence required varying the global mesh sizes of the sub model and obtaining the corresponding maximum stresses (Von Mises) and trends of the converging started at 2.3 mm as shown in Table 7. Further decrement of the size would only increase computational time with minimal change in the stresses.

Table 7: *Global Mesh Size and obtained stresses*

Global Mesh size (mm)	Number of Elements	Number of Nodes	Von Mises (MPa)
7.0	21463	99686	155

6.0	33032	150588	158
5.0	53772	240283	169
4.0	100016	438490	270
3.0	427081	655742	449
2.9	438050	674090	456
2.7	507850	778850	470
2.5	592460	909000	473
2.3	649270	996050	533
2.1	694090	1064700	585
1.9	763330	1169800	589

3.6 Validation

The results from the analysis in ANSYS are to be validated against experimental and/or literature reviews to ensure accuracy and relevance. Relative variation is measured and optimization is performed on the CAD models to bring the variation to an acceptable percentage (<5%).

3.7 Fatigue Analysis with FRANC3D

The procedure follows 5 detailed steps as listed below

- *Crack insertion*

  This involves positioning and orienting of the semi-elliptic crack at the location at which maximum Von Mises stress were found within the un-cracked model.
- *Static analysis of the cracked model*

  The model database from the previous step is then analyzed using the ANSYS-code features within the software.
- *Computation of the Stress Intensity Factors (SIF, K)*

  Tools within the software are used to compute for the related *K* values at the various crack fronts.
- *Crack growth analysis*

The analysis follows insertion of the necessary parameters related to the chosen crack growth algorithm (Paris' law) and automation of the growth process using at least sopping criteria, that is, change in K threshold value; K being greater than the critical value; all data in spt file. The *crack growth history* file is created within the software and saved for extraction of related *K* history with the crack grown.

- *Fatigue life cycle prediction*

  The parameters related to the fatigue life computation, such as *C* and *n*, are input as required into the analysis environment following the crack's initial length. The software then computes the related life cycles and final crack length based on the availed data.

The crack growth automated analysis gives a 'K vs a' curve as an SIF Path file (.spt) file that is imported into the fatigue analysis environment for life cycle computation as related to the curve data. The data in the curve is a representation of the information at the crack fronts as transformed into a single DOF model by the software then combined using a crack growth rate model (equation $N= \int \frac{da}{f(\Delta K,R,\Delta K_{th},\dots)}$ … **viii**) for the life cycles. The cycles are highly affected by path file (.spt).

$$N = \int \frac{da}{f(\Delta K,R,\Delta K_{th},\dots)} \quad \dots \textbf{\textit{viii}}$$

3.8 Research Model

The study implements a 3-Dimensional wheel/rail contact system with a 30^0 sectioned wheel and 200mm rail to analyze the region of maximum stress (Von Mises) and a further sectioned wheel (around the region of maximum stress) with a crack included and oriented in the direction of motion (X) to capture opening stresses from forward motion, the vertical direction (Y) to check the effects of subsurface tensile-compressive stress gradients to the tread surface stresses, and the lateral direction (Z) to reveal mixed-mode and shear effects. This not only determines the stress distributions and effects due to the cracks but also the behavior of cracks under mixed-mode loading and the fatigue life cycles due to the variation of the crack lengths.

Chapter 4: Results and Discussion

This section includes the results obtained from the static analysis from ANSYS, validation, and crack analysis using FRANC3D tools. Results from the simulations from ANSYS with variations in the loading based on the rated and overload capacities; orientations of the crack based on the vertical, lateral, and longitudinal directions to investigate their effect on the stress distributions at the tread surface; fatigue life cycles and crack growth rates from the Fracture analysis software.

A vertical load equivalent to the W_R and W_O is applied to the wheel section. For standardization of the analysis, the refinement level 2 was added as a mesh control mechanism on the contact, the rotation of the wheel was neglected, and a flat and straight path is considered hence rendering the lateral forces to Zero, a friction coefficient of 0.3 was used to ensure that the model captures the highest possible tangential forces at the wheel-rail interface that could yield worst-case stresses onto the tread.

4.1 Model results comparison

The trends, as represented in Figure 17, in the mesh convergence for this study are similar to those of Tesfaye et al. [44] while they determined the optimal mesh size that yielded accurate results without incurring excessive computational time. The Maximum Von Mises stress (589 MPa) obtained from the sub-model of the wheel and rail contact interface highly agrees with that of 614MPa as obtained in the work of Garcia et al. [45] using a force of 50kN.

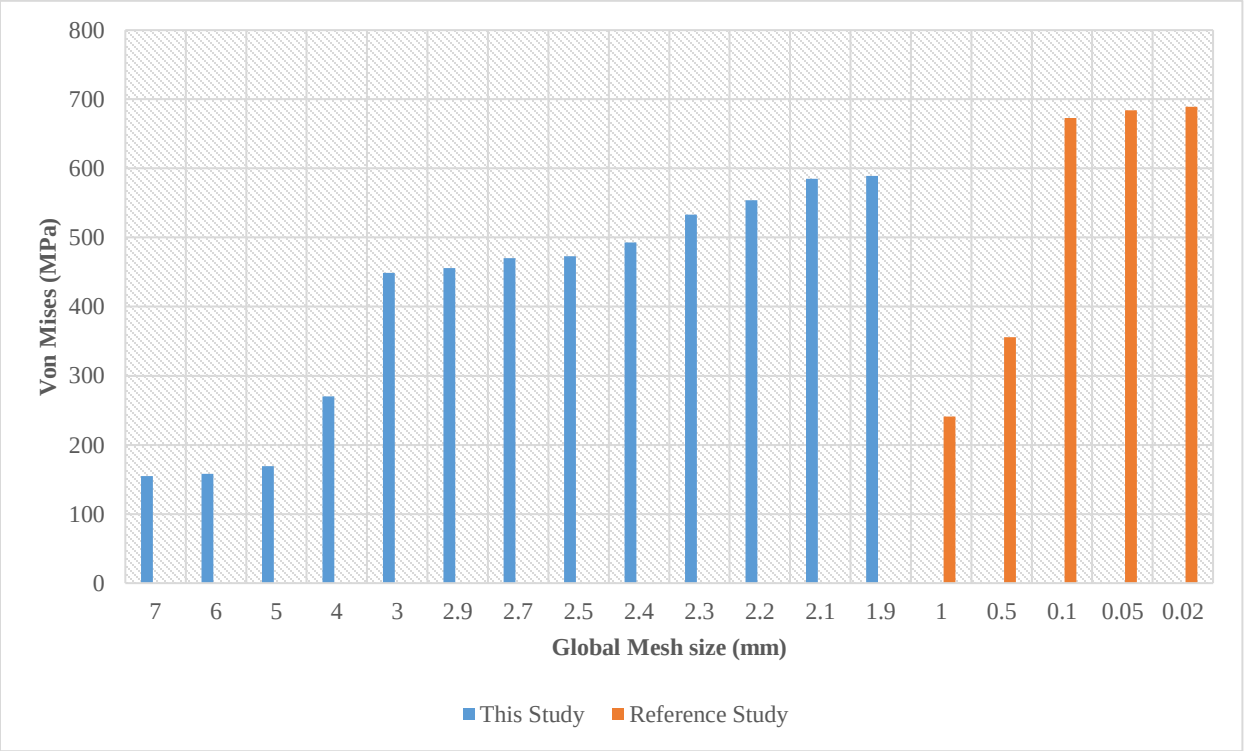

Figure 17: Results comparison

Given the modeling assumptions made, the small discrepancy (4.2%) falls within the acceptable range as mentioned in *section 3.6* of this paper. Therefore, the FE-model was deemed sufficiently reliable for the further analyses and design work that depend on it.

4.2 FEA (ANSYS) Results

Here included are the stress (Von Mises) results obtained from varying the loading conditions, that is, rated and overload capacities. Equation $Using\,Weight, W = mg$ ***…ix*** was used for evaluating the vertical load (Force) used in the analyses.

$$Using\ Weight, W = mg \qquad \textbf{…ix}$$

Referring to Table 6, and taking$g = 9.81 m/s^2$; let $\boldsymbol{W_R}$ and $\boldsymbol{W_O}$ be the rated weight and overload weight respectively; and $\boldsymbol{m_r}$ and $\boldsymbol{m_o}$ be the rated and overload masses.

$$m_r = \frac{10 \times 1000}{2} = \mathbf{5000kg}$$

$$\boldsymbol{W_R} = 5000 \times 9.81 = \mathbf{49050N} \equiv \mathbf{49.05kN}$$

$$m_o = \frac{11 \times 1000}{2} = \mathbf{5500kg}$$

$$\boldsymbol{W_O} = 5500 \times 9.81 = \mathbf{53955N} \equiv \mathbf{53.955kN}$$

A global mesh size of 2mm (Figure 18) with 726,269 elements and 1,113,353 nodes was used for the simulations.

Table 8: *Axle and wheel loads*

	Axle load (t)	Axle load (kN)	Load at wheel (kN)
Empty	7	70	34.3
Rated passenger capacity	10	100	49.05
Overload passenger capacity	11	110	53.955

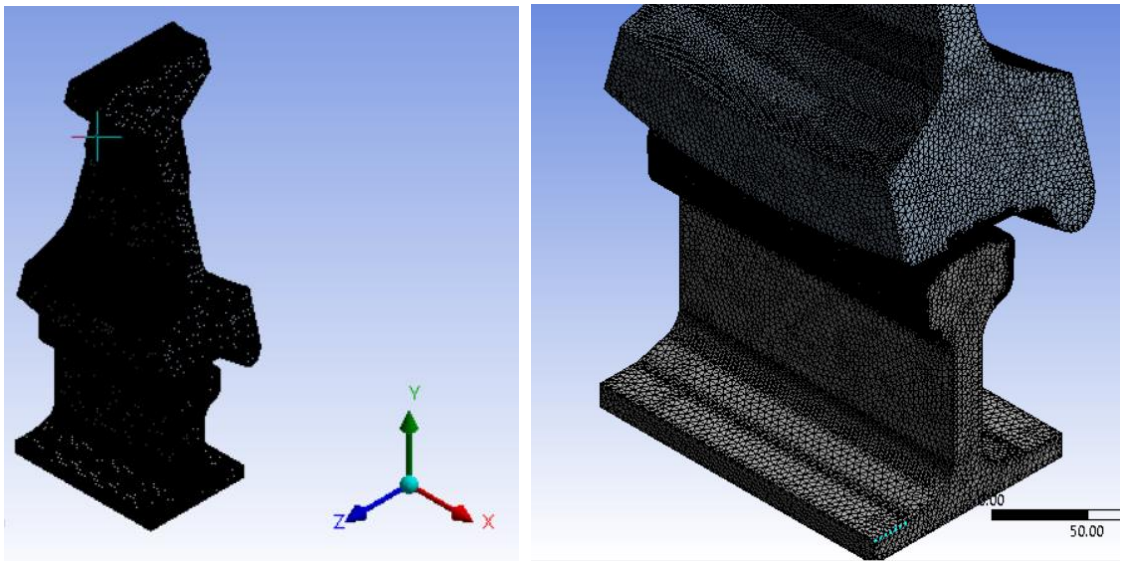

(a) (b)

Figure 18: *(a) Meshed model; (b) Zoomed view of the meshed model*

Stress results are reported in terms of the following cases:

- Case I: Rated capacity

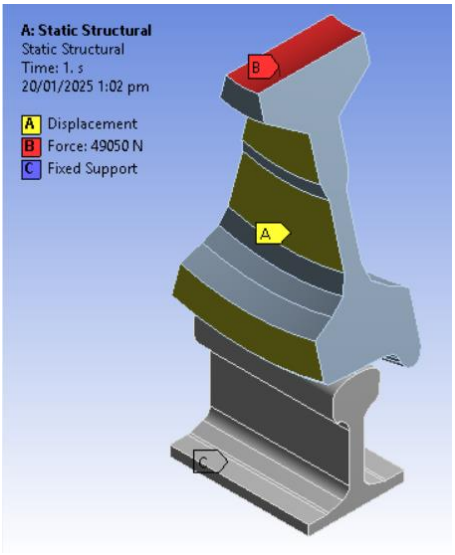

Figure 19: *Case I loading conditions*

  - Case I_0: Rated capacity; Zero crack formation
  - Case I_x: Rated capacity; Longitudinal crack orientation
  - Case I_y: Rated capacity; Vertical crack orientation
  - Case I_z: Rated capacity; Lateral crack orientation
- Case II: Overload Capacity

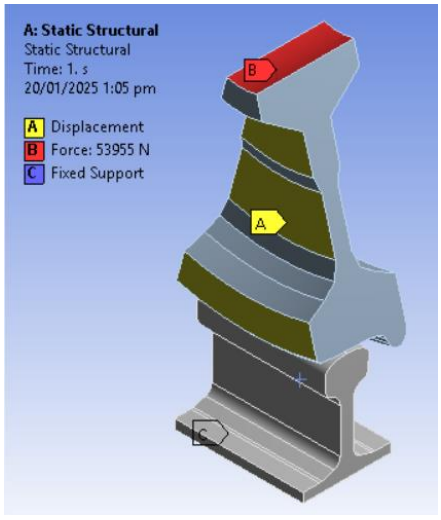

Figure 20: *Case II loading conditions*

  - Case II_0: Overload capacity; Zero crack formation

- Case II_x: Overload capacity; Longitudinal crack orientation
- Case II_y: Overload capacity; Vertical crack orientation
- Case II_z: Overload capacity; Lateral crack orientation

4.3 Stress Distribution Results

The simulations were run with the mesh files imported between ANSYS (for stress analyses) and FRANC3D (for crack insertion and updated model meshes). The sectioned views presented in this section were made from sectioning the wheel model after analysis, from the X and Z directions.

Case Io:

The wheel tread surface experienced a maximum stress of 578 MPa, which is notably lower than both the yield and ultimate strength values of the wheel material. This demonstrates that the wheel can operate safely under normal load without experiencing structural degradation as shown in Figure 22 and Figure 23.

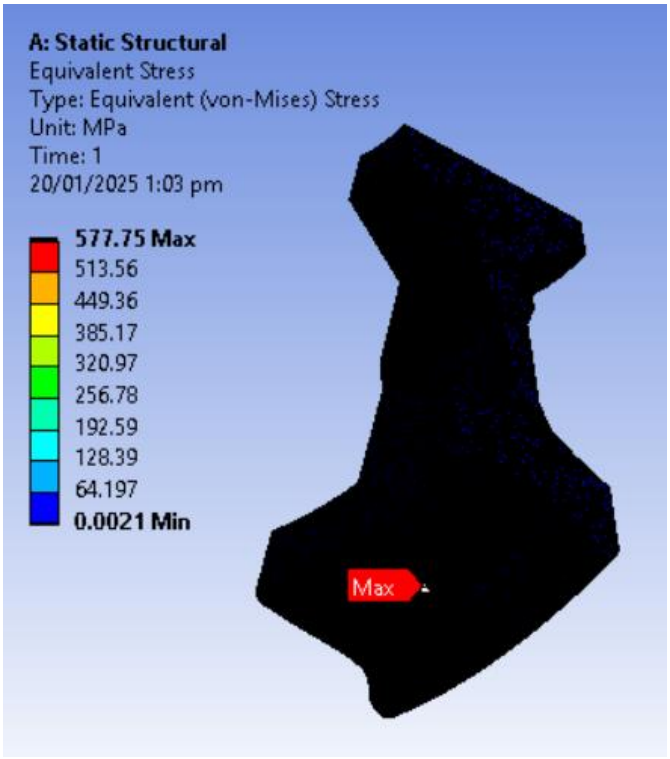

Figure 21: *Case Io Maximum surface stress at wheel tread*

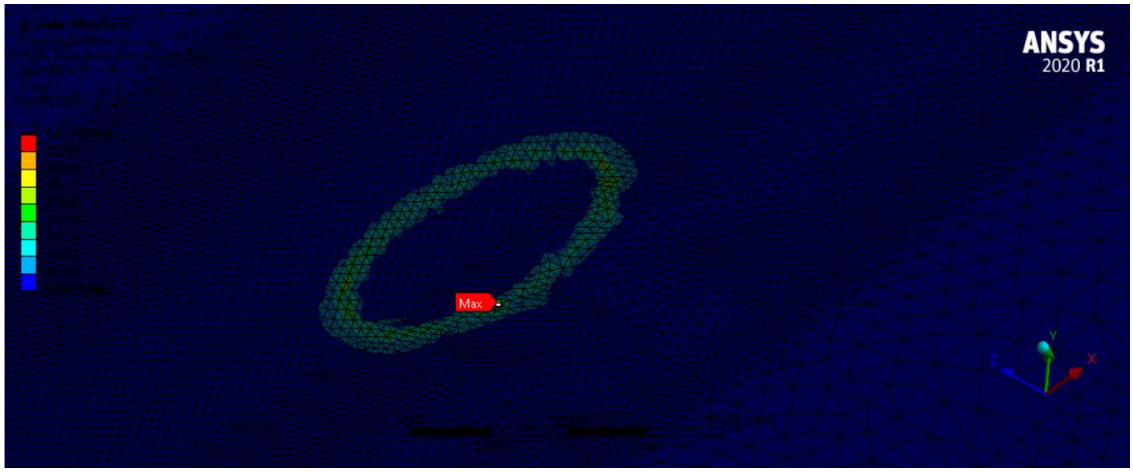

Figure 22: *Case Io Maximum surface stress at wheel tread (Zoomed)*

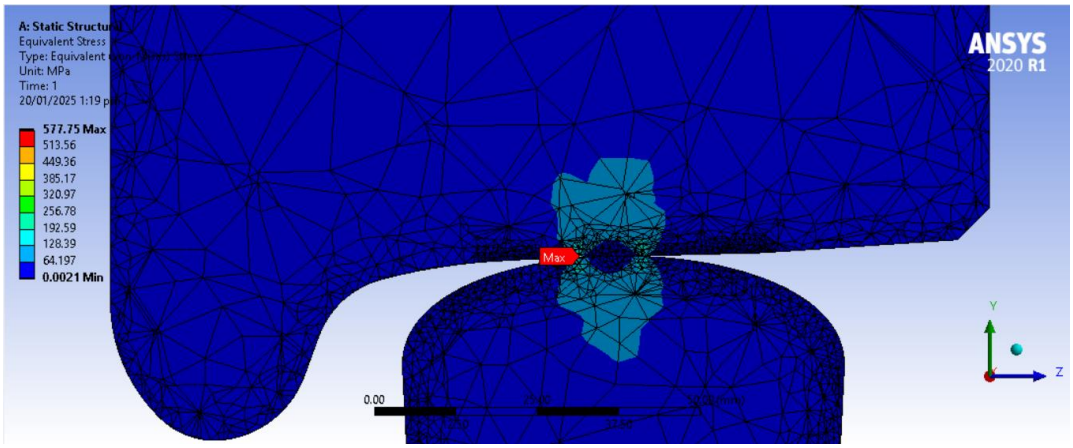

Figure 23: *Case Io Maximum surface stress at wheel/rail contact (X-plane sectioned view)*

Case Ix:

A crack positioned along the direction of wheel motion, under rated conditions, resulted in a substantial increase in stress, peaking at 1225 MPa as represented by the scale on the left in Figure 24. This value significantly exceeds the ultimate tensile strength of the material, indicating a serious risk of sudden crack propagation and potential failure.

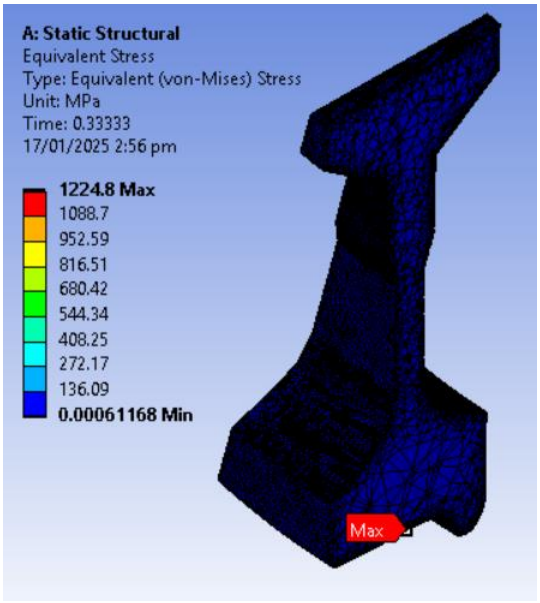

Figure 24: *Maximum surface stress at wheel/rail contact (sectioned view)*

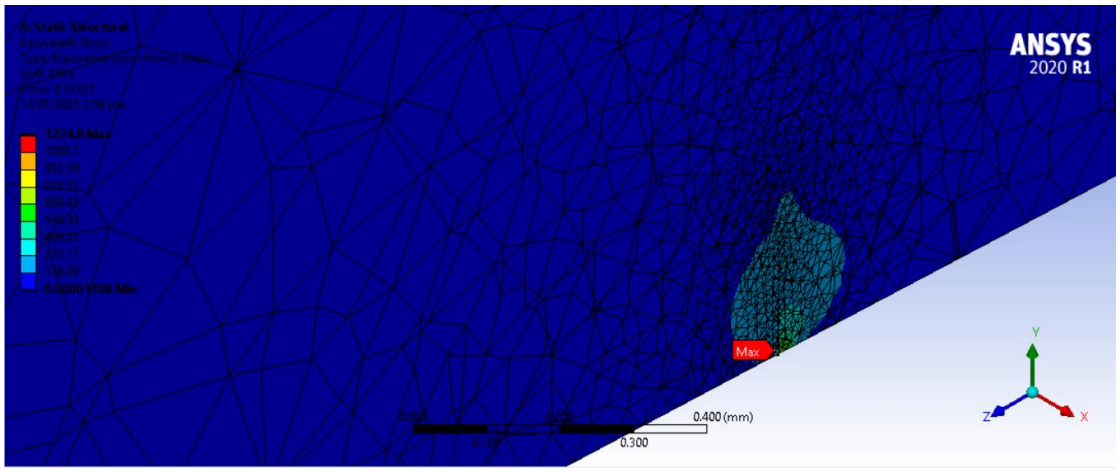

Figure 25: *Maximum surface stress at wheel/rail contact (Zoomed X-plane sectioned view)*

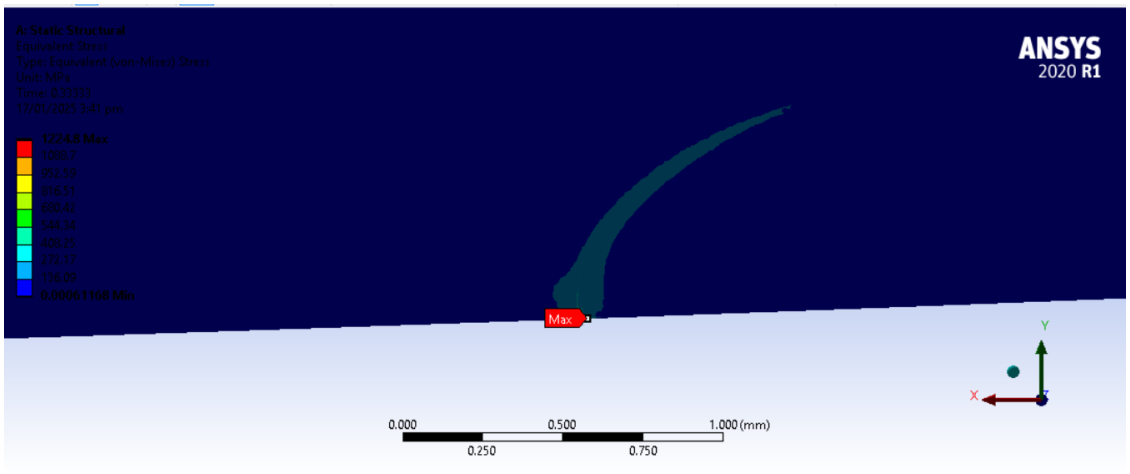

Figure 26: *Maximum surface stress at wheel/rail contact (Z plane sectioned view)*

Case Iy:

The maximum stress rose to 782 MPa. While still within the material's failure threshold, this marks a substantial increase compared to the un-cracked scenario. Such a crack alignment leads to a moderate stress rise, suggesting that fatigue progression would be gradual, but persistent

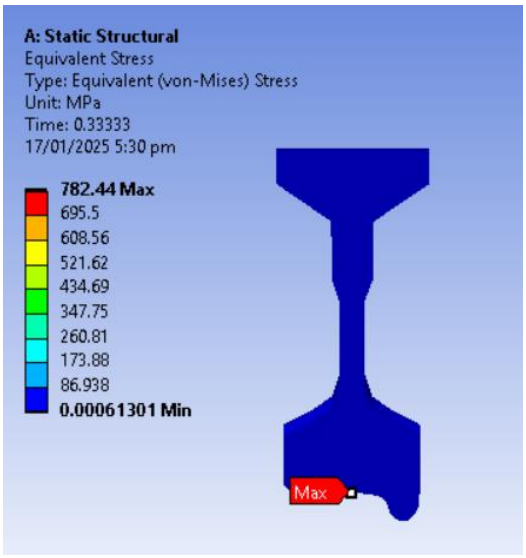

Figure 27: *Maximum surface stress at wheel/rail contact (X plane sectioned view)*

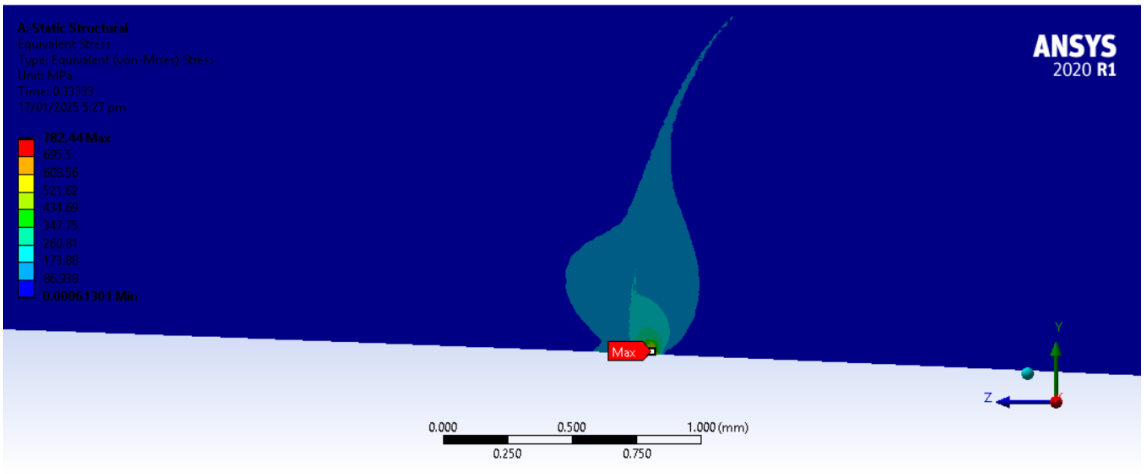

Figure 28: *Maximum surface stress at wheel/rail contact (X plane sectioned view)*

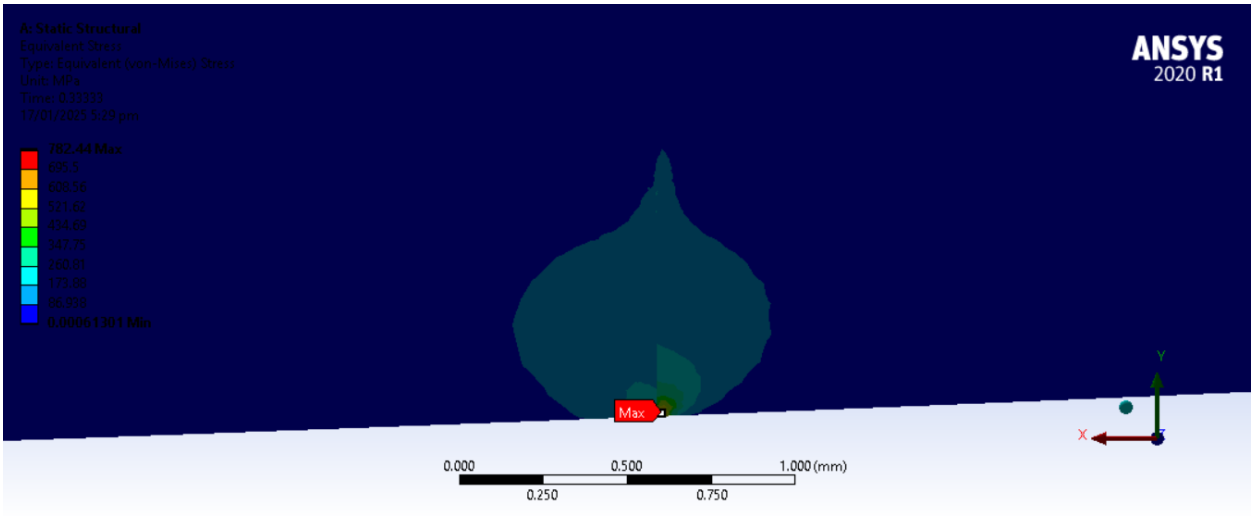

Figure 29: *Maximum surface stress at wheel/rail contact (Z plane sectioned view)*

Case Iz:

A laterally oriented crack caused the stress to reach approximately 770 MPa. This stress level mirrors the result from the vertical crack orientation (case Iy), implying a comparable level of concern.

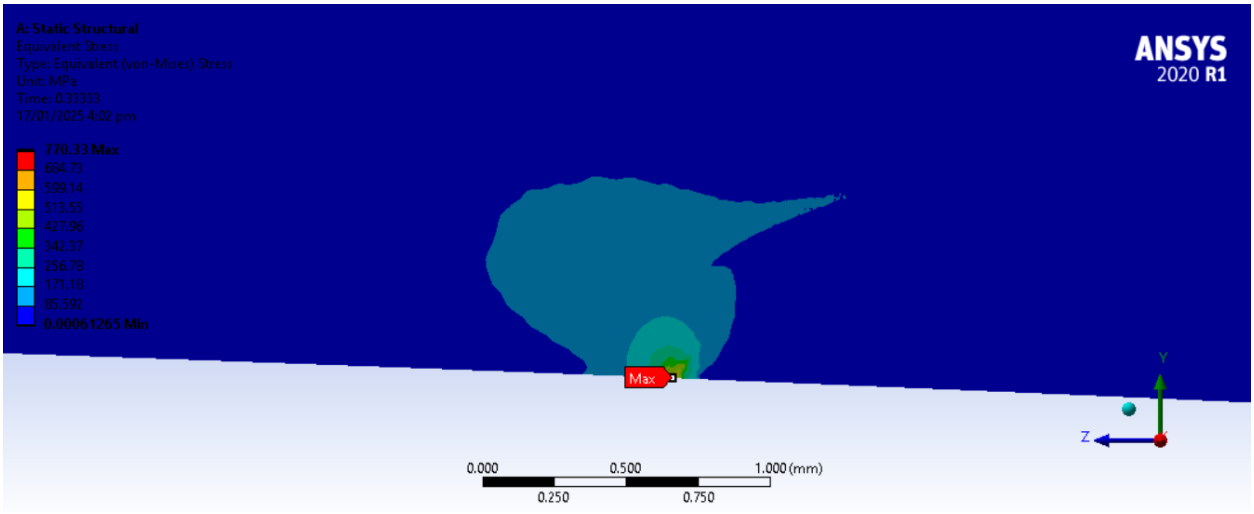

Figure 30: *Maximum surface stress at wheel/rail contact (X plane sectioned view)*

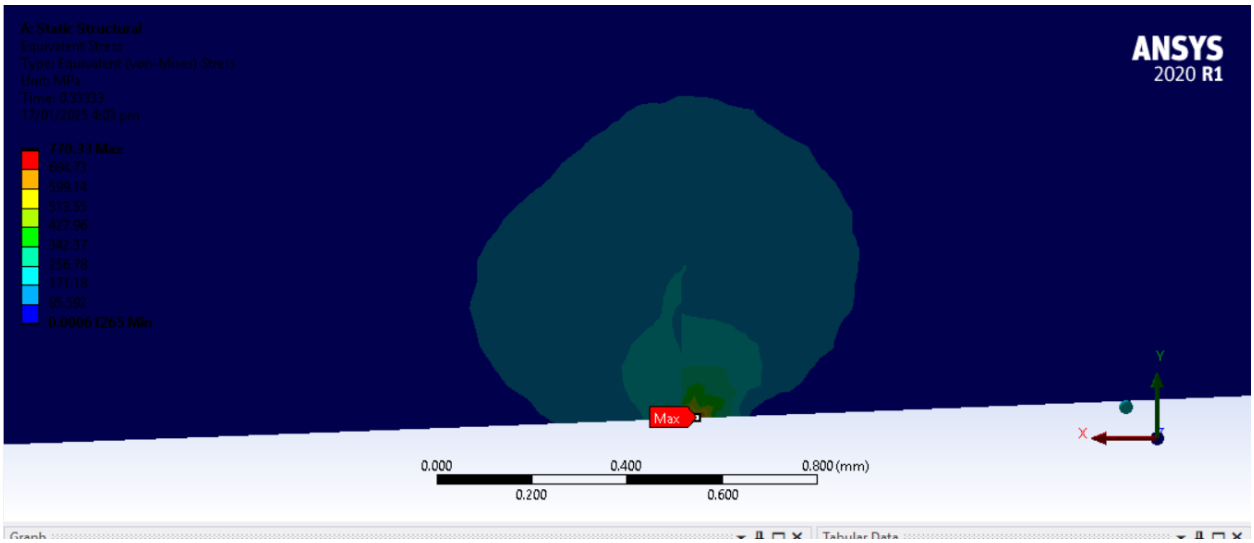

Figure 31: *Maximum surface stress at wheel/rail contact (Z plane sectioned view)*

Case IIo:

With the system subjected to overload conditions and no cracks introduced, the resulting stress increased to 636 MPa. Though this value is still under the material's ultimate limit, the rise compared to the rated load scenario highlights how stress scales with increased loading.

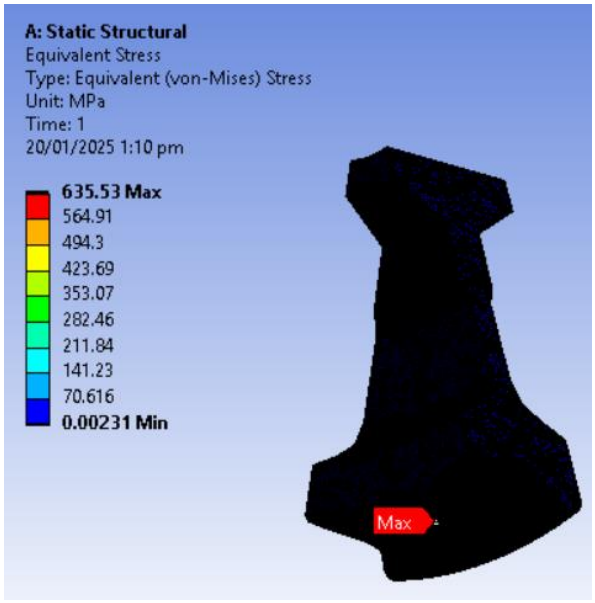

Figure 32: *Case II Maximum surface stress at wheel tread*

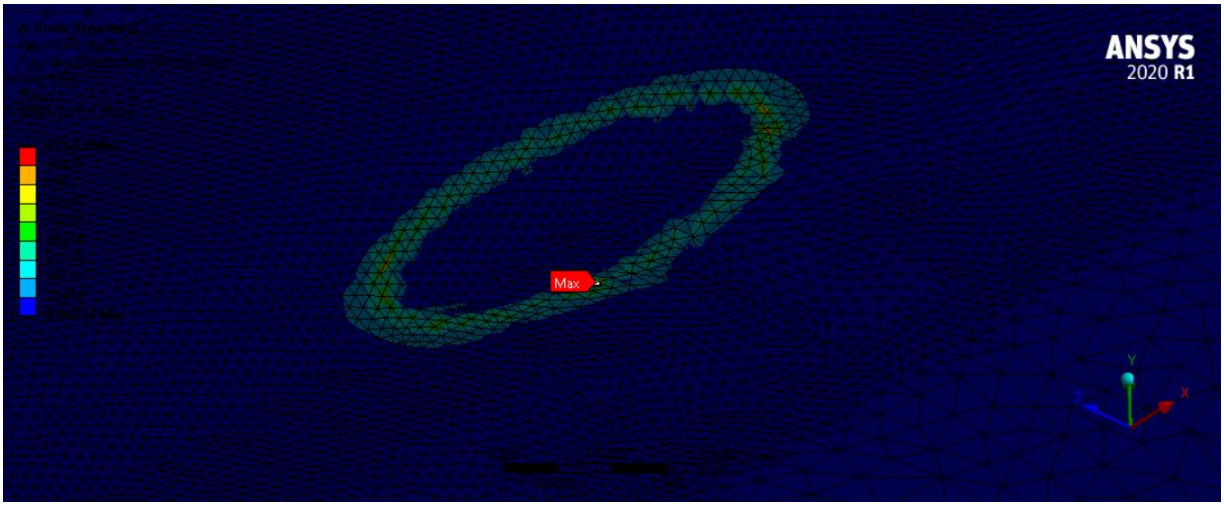

Figure 33: *Case II Maximum surface stress at wheel tread (Zoomed)*

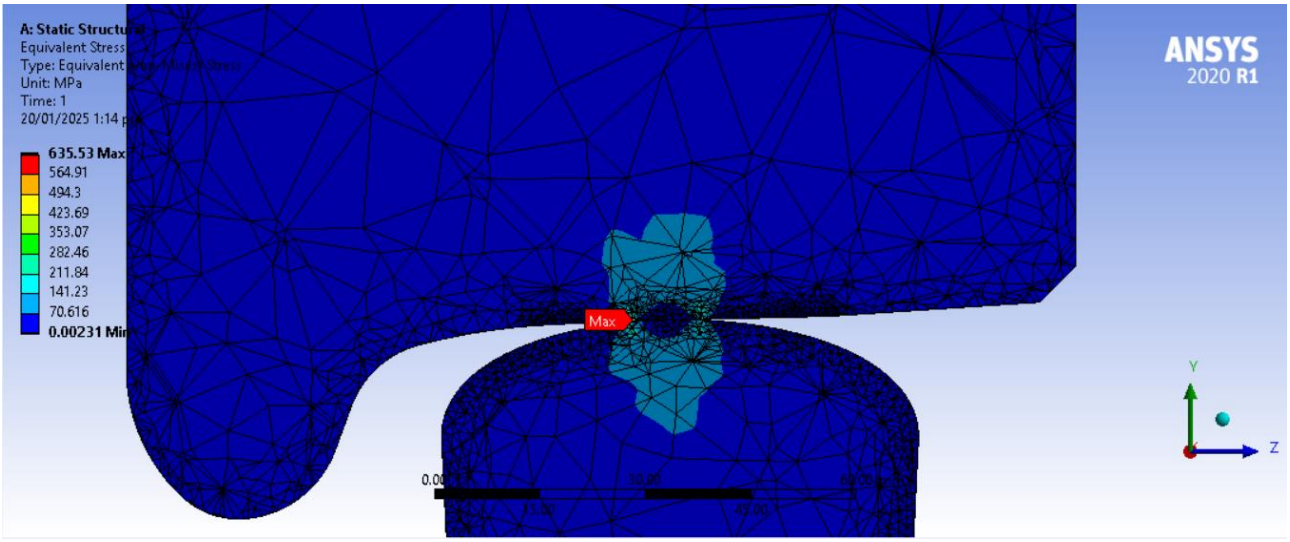

Figure 34: *Case I Maximum surface stress at wheel/rail contact (X-plane sectioned view)*

Case IIx:

When both overload and a crack oriented in the motion direction are present, the highest surface stress recorded was 1347 MPa. This value far exceeds the material's capacity to withstand stress, which may also be an indicator for imminent failure.

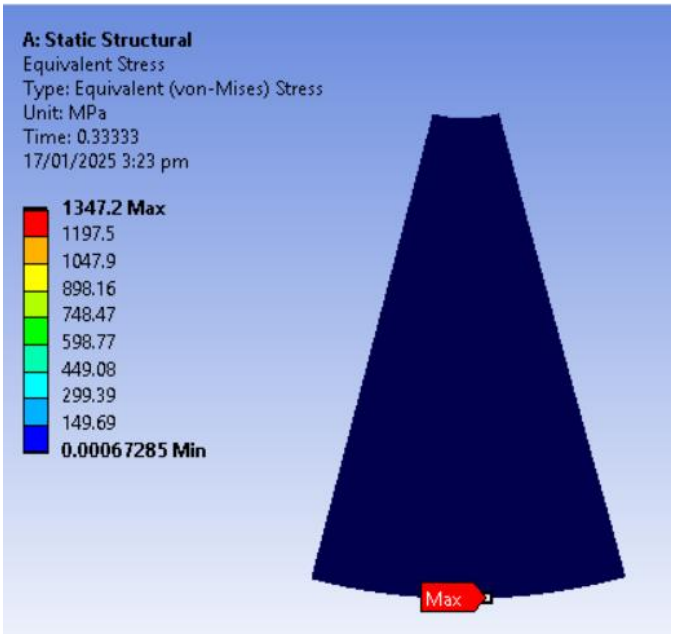

Figure 35: *Maximum surface stress at wheel/rail contact (X plane sectioned view)*

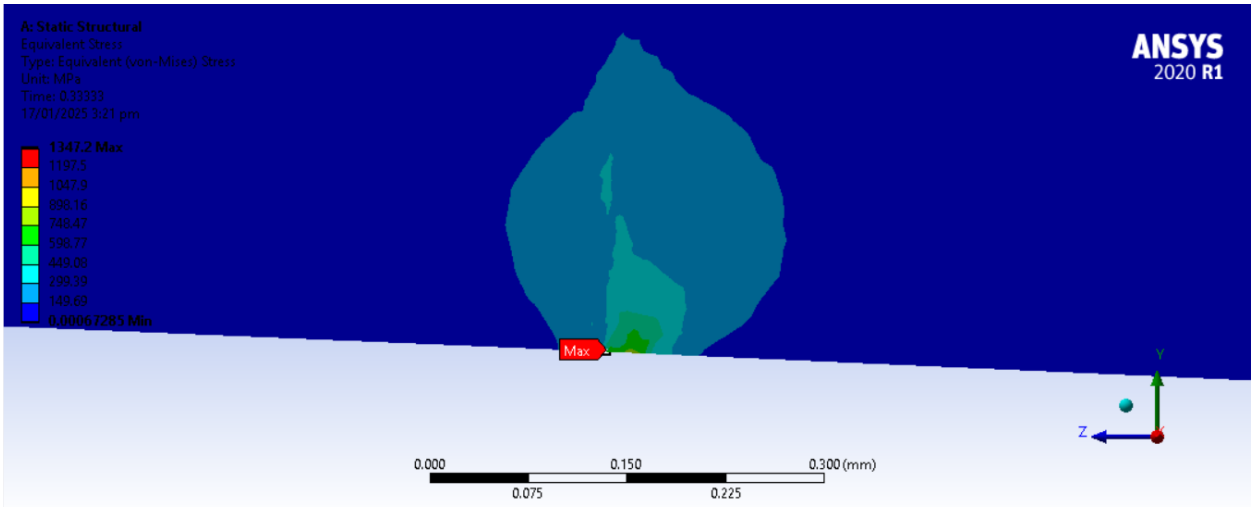

Figure 36: *Maximum surface stress at wheel/rail contact (X plane sectioned view)*

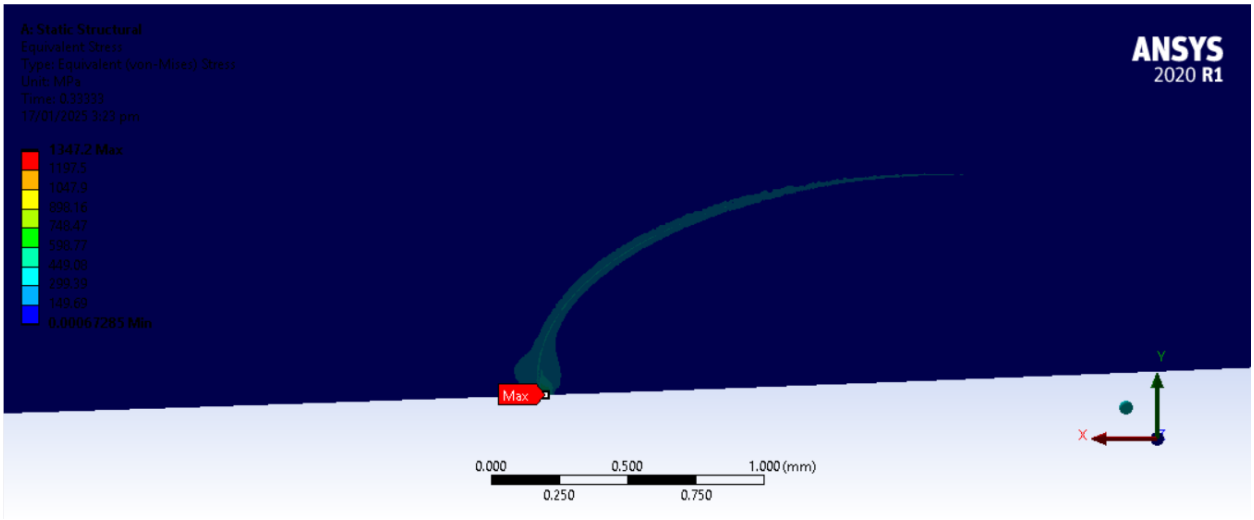

Figure 37: *Maximum surface stress at wheel/rail contact (Z plane sectioned view)*

Case IIy:

The surface stress levels reached 860 MPa; very close to the wheel's tensile strength limit. Although not yet in failure territory, this scenario suggests that the component is operating near its critical threshold.

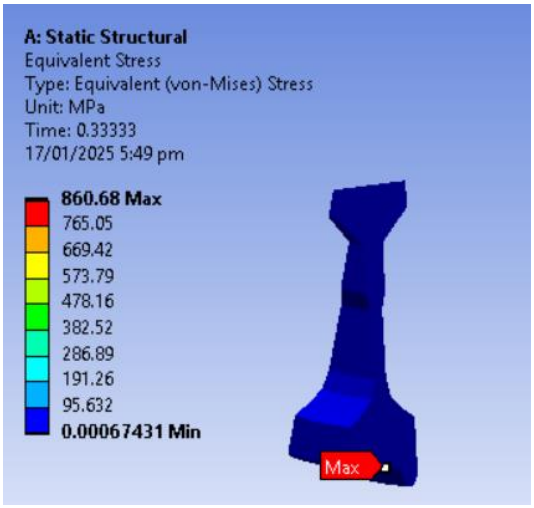

Figure 38: *Maximum surface stress at wheel/rail contact (sectioned view)*

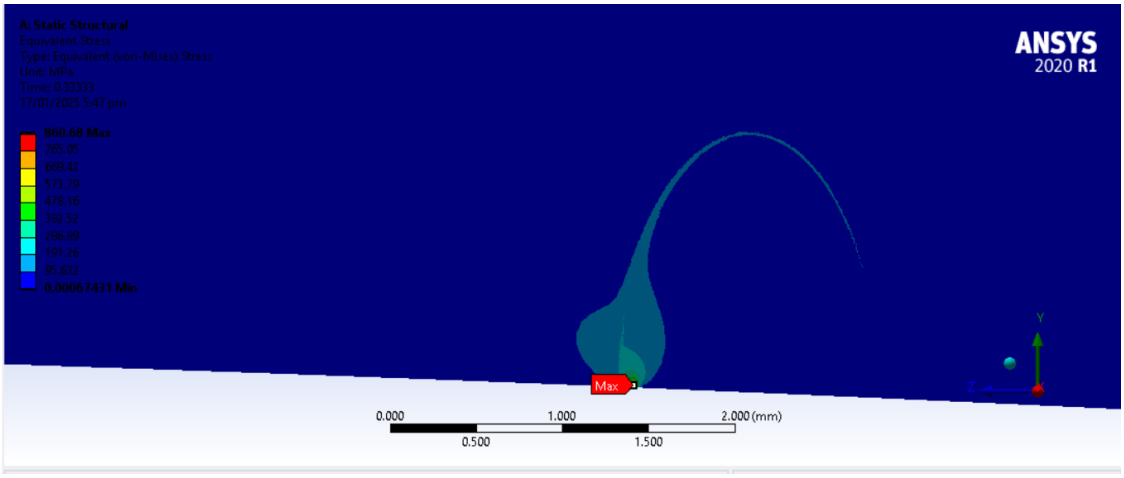

Figure 39: *Maximum surface stress at wheel/rail contact (X plane sectioned view)*

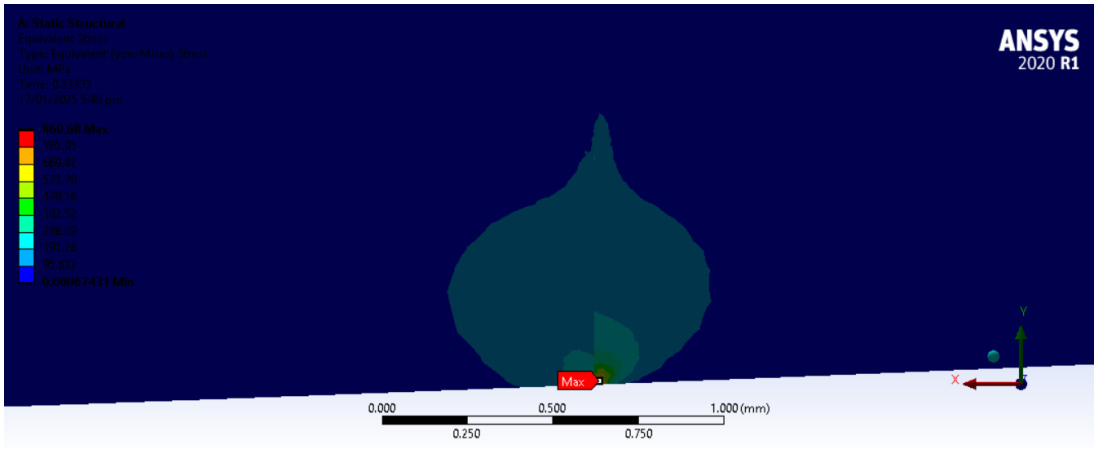

Figure 40: *Maximum surface stress at wheel/rail contact (Z plane sectioned view)*

Case IIz:

The resulting surface stress was approximately 847 MPa. This value, while slightly below the vertical case (case IIy), still places the wheel tread material close to its limit.

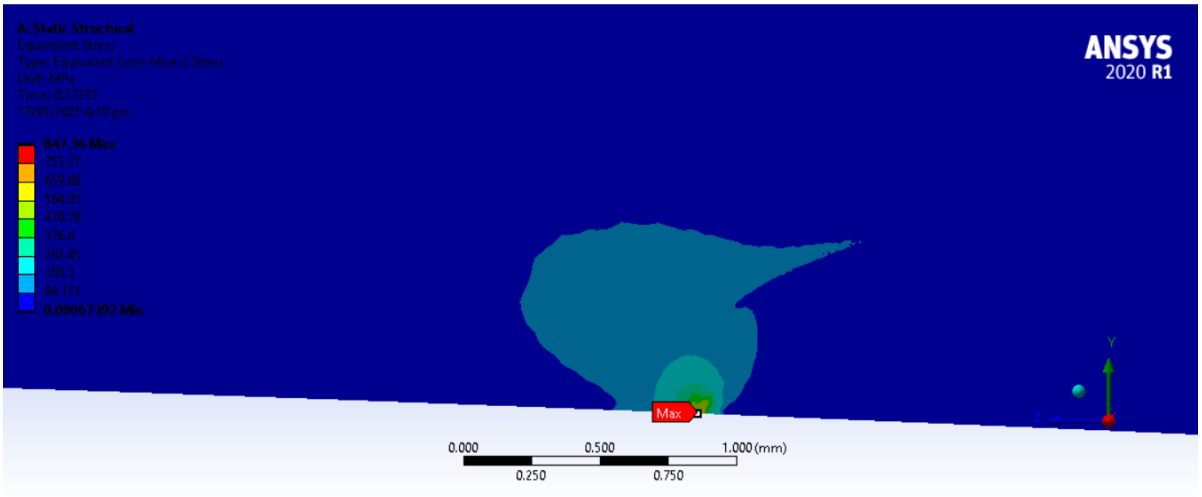

Figure 41: *Maximum surface stress at wheel/rail contact (X plane sectioned view)*

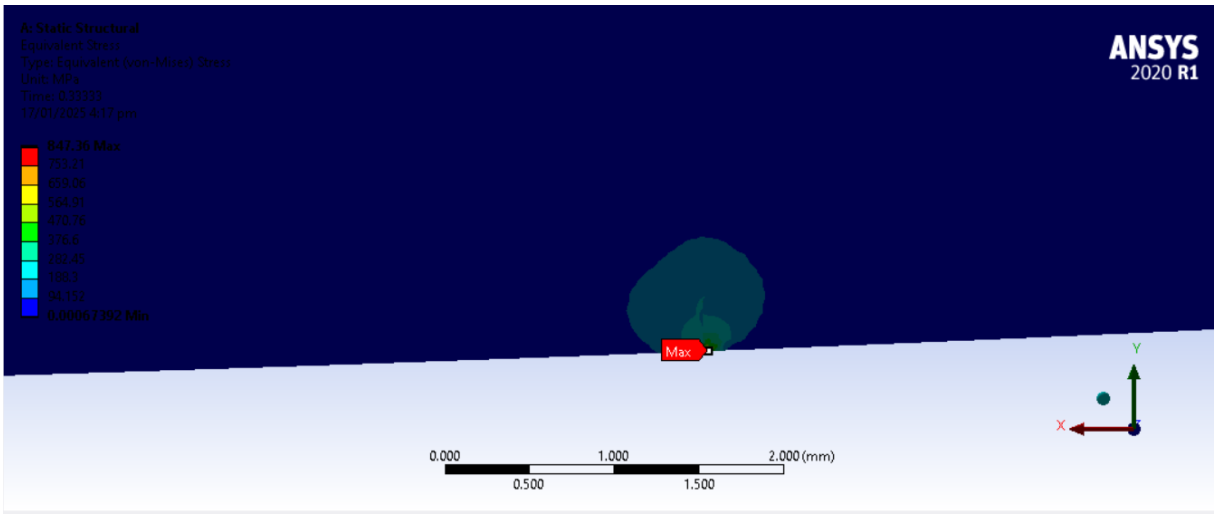

Figure 42: *Maximum surface stress at wheel/rail contact (Z plane sectioned view)*

The maximum stress (Von Mises) at the cracked wheel tread surface was found with the crack oriented in the direction of motion, that is, the X-direction as shown in Figure 43. This was the observed in both loading cases (rated and overload).

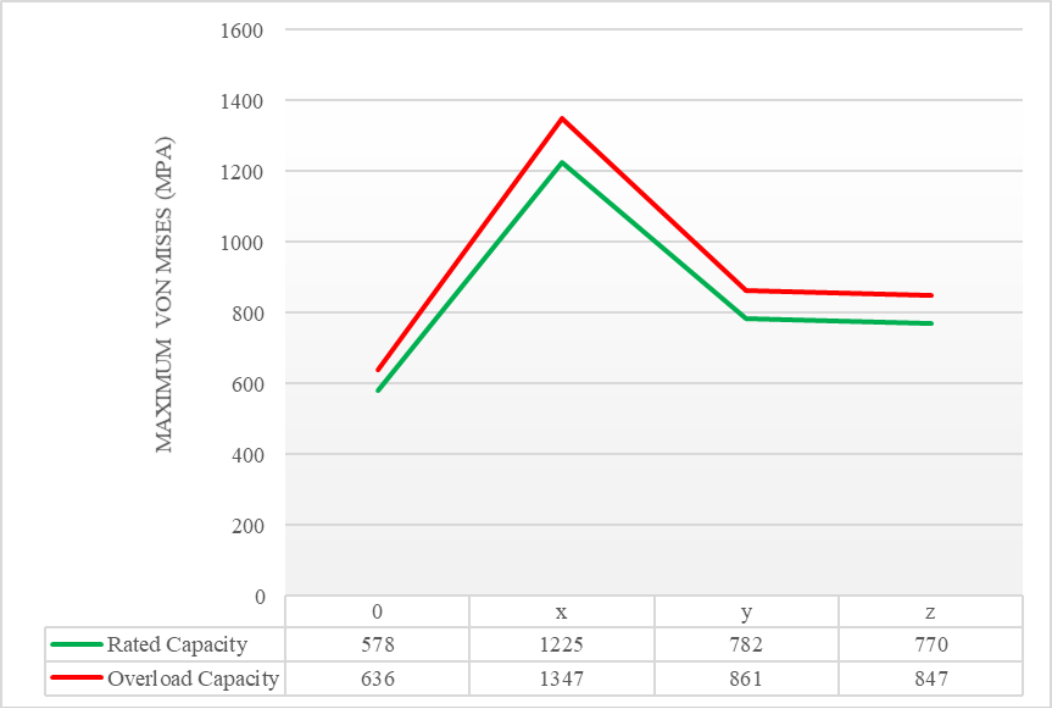

Figure 43: Maximum stress (Von Mises) with no crack and with different crack orientations

Besides cases *Ix* and *IIx*, all the other showed increase on the maximum tread surface stress but with values below the ultimate tensile strength of the material of the wheel. These cases (*Ix* and *IIx*) showed stresses beyond 879MPa (ultimate tensile strength of the used wheel material), that is, 1225MPa and 1347MPa, respectively.

To note, the approximate calculated variation between the cases with rated and overload capacities was found to be 10%. This variation also showed that the model was capturing the sensitivity to load variations as anticipated.

4.4 Fatigue results

The results presented in this section are based on the steps as explained in *section 3.7* of this document. From the general coordinate system used for the un-cracked model in ANSYS Mechanical, the crack was anchored at the node within the region of maximum stress at the wheel tread surface with coordinates *X = 99.06mm, Y = 185.68 mm, Z = 116.74mm* as shown in Figure 44.

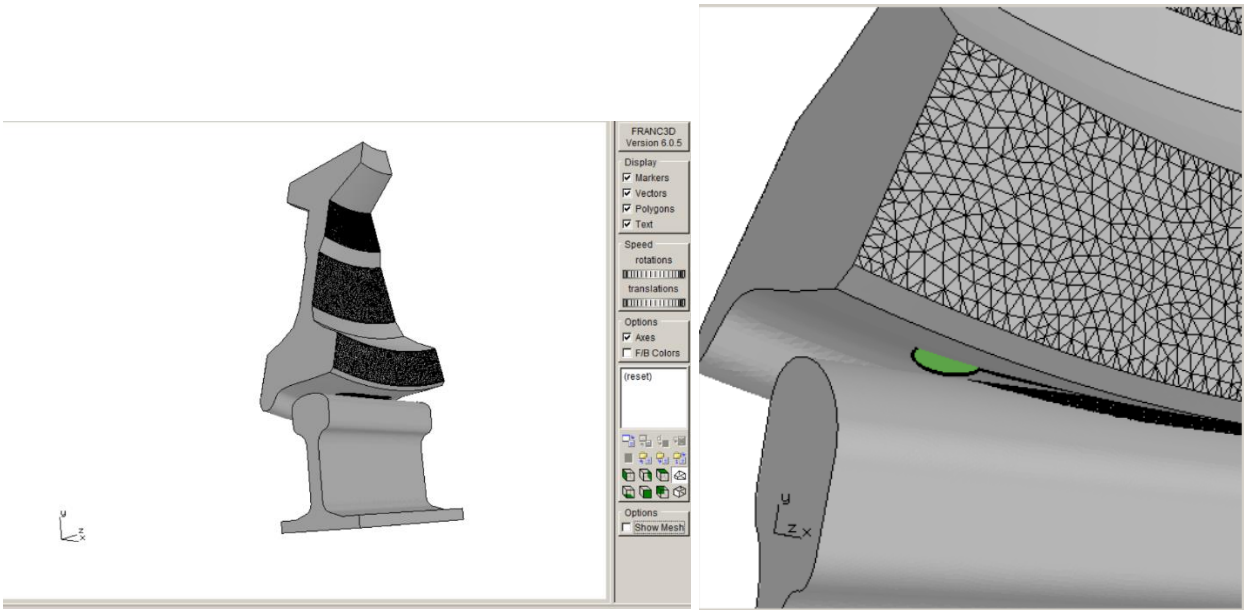

Figure 44: *Imported mesh file (Left) and crack insertion (Right)*

The results were obtained from the fatigue analysis with the crack length varied (0.75mm, 1.05mm, and 1.35mm) but oriented in the direction of motion (the case where maximum stresses obtained were above the wheel's ultimate tensile stress). 2 stopping criteria were applied, that is, *K vs a* plot data from the analysis steps and critical SIF, K_{IC} for the wheel material. K_{IC} used in the analyses was$1581 MPa\sqrt{mm}$.

4.4.1 K-Mode analysis

The Figure 45 illustrates the dominance of Mode I stress intensity factor (KI) across the crack front during loading, while Mode II (KII) and Mode III (KIII) contributions remain minimal. This trend confirms that the primary crack-driving force in the wheel tread is opening-mode fracture, consistent with tension-dominated regions under vertical loading. The minimal influence of shear modes highlights that crack growth is governed primarily by normal tensile stress rather than in-plane or out-of-plane shear. This suggests that fatigue progression is likely to follow a path perpendicular to the surface rather than deviating along the wheel contour.

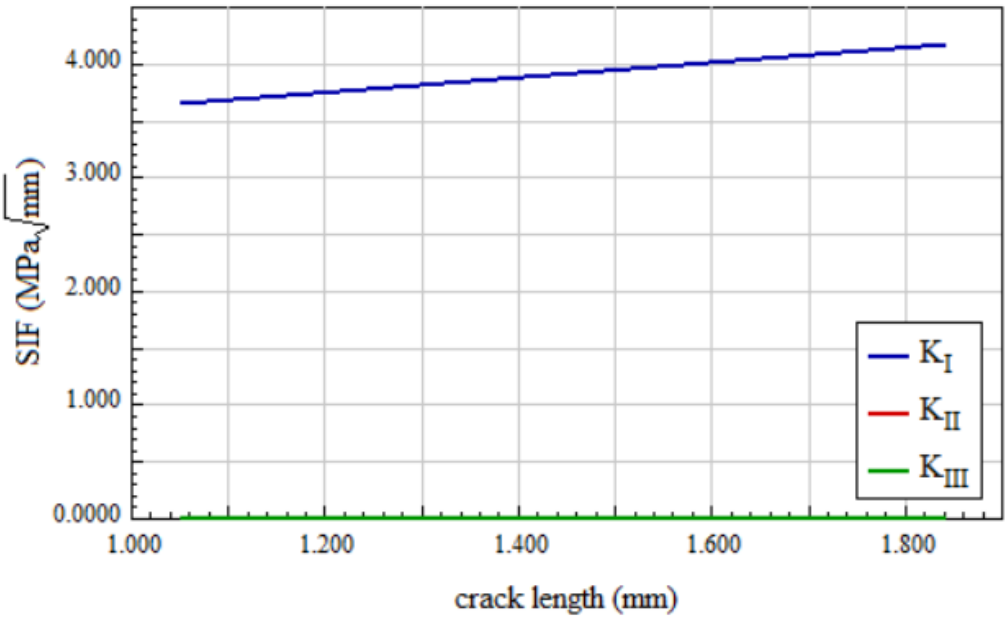

Figure 45: *Dominance of K_I over K_{II} and K_{III}*

4.4.2 Crack length variation

For the smallest initial crack (0.75 mm), the graph in Figure 46 shows a relatively slow progression toward failure, as reflected by the rise number of fatigue cycles.

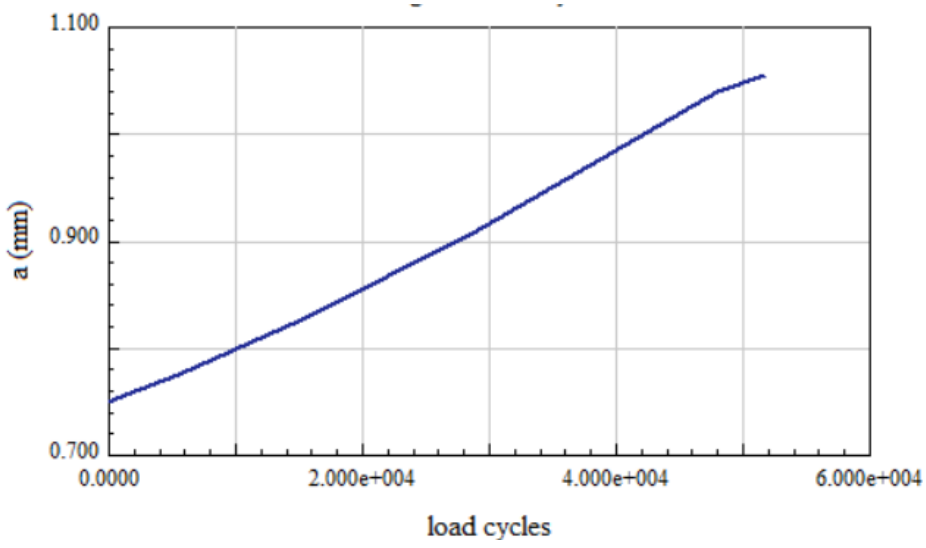

Figure 46: *Life cycles from S_1*

This indicates a phase of stable crack growth, where the material resists rapid propagation, likely due to low local stress intensity. The fatigue life in this scenario exceeds 9.8 million cycles, suggesting that early-stage cracks may persist for extended durations before becoming critical.

As the initial crack length increases to 1.05 mm, the number of life cycles to failure drops significantly as in Figure 47.

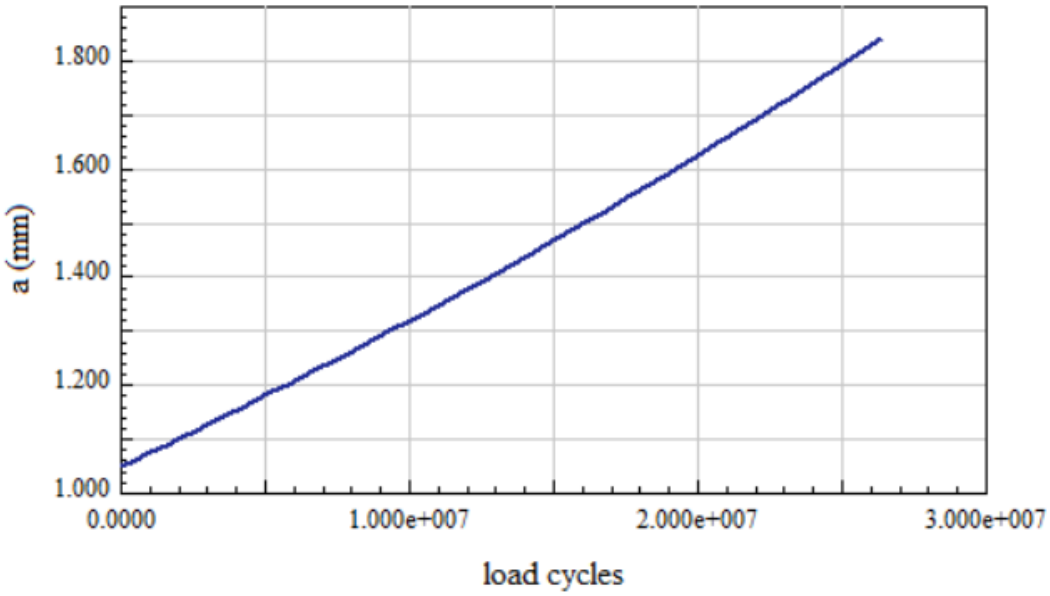

Figure 47: *Life cycles from S_2*

This shift marks the onset of accelerated crack growth, likely due to higher effective stress intensity. Compared to the first scenario, there is a noticeable reduction in resistance to crack propagation, signaling that mid-sized defects have greater sensitivity to cyclic stress.

For the largest initial crack analyzed (1.35 mm), the fatigue life cycles drops still. The number of cycles before failure becomes nearly equivalent to that of the smaller cracks despite a much larger starting defect, suggesting that the crack has entered a critical instability phase represented by the steepness in Figure 48.

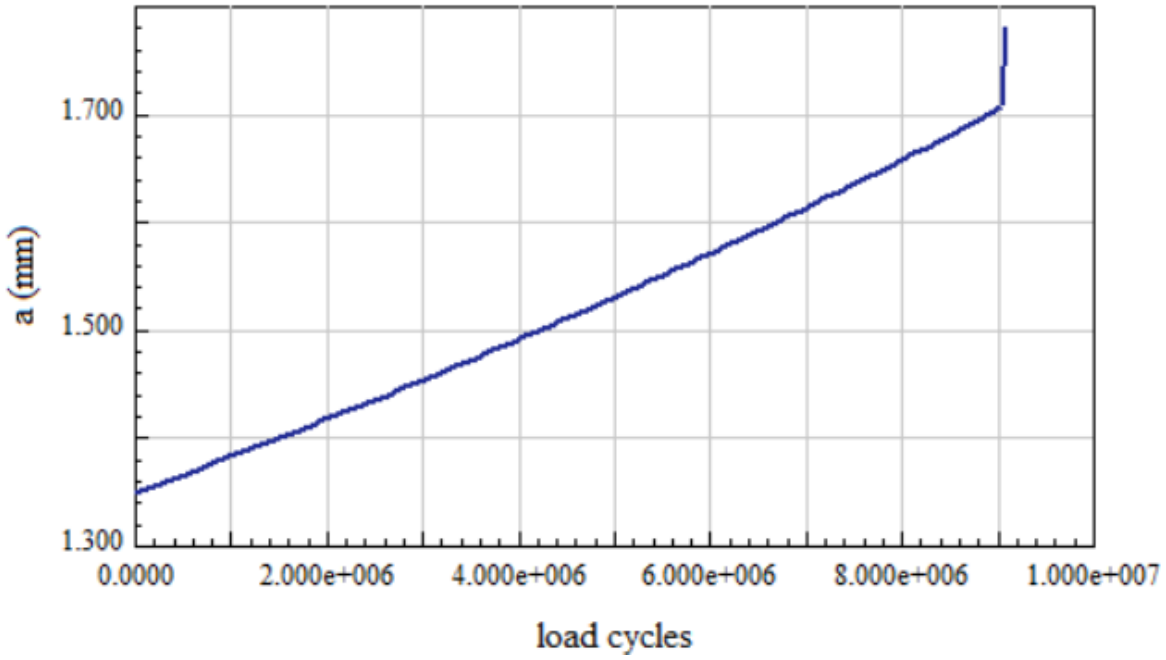

Figure 48: *Life cycles from S_3*

The significant reduction in cycles implies that once cracks grow beyond a certain threshold, the wheel material quickly loses its ability to arrest further propagation, pushing it into a high-risk state of imminent failure.

Table 9: *Results comparison from the fatigue analysis*

	S_1	S_2	S_3
a_i	0.75	1.05	1.35
a_f	1.05495	1.84377	1.77982
a_m	-	-	1.94032
Δa	0.305	0.794	0.430
N_e	9882046	26397136	9088677
$C/mm.G$	32×10^6	33×10^6	21×10^6

The results in Table 9 show that at S_1 and S_2, computed values lie with acceptable ranges ($K \leq K_{IC}$) relative to the set stopping criteria. The drop in the cycles between S2 and S3 implies an unstable crack growth as further shown in the drastic change in the *C/mm.G*. However, at S_3, *K vs*

a, the maximum crack length achieved is 1.94032mm; however, $K>K_{IC}$, therefore, suggesting a failure rendering the model invalid due to material failure. The overshoot in the recorded K-value in S_3 suggested more abrupt failure scenarios.

As the value of *C/mm.G* lowers (indicating a reduction in the material's resistance to crack growth), the number of cycles to failure also reduced significantly.

4.4.1 Fatigue results comparison

The fatigue life results obtained in this study agreed with those from the work of Masoudi et al. [46] emphasizing decrease of fatigue life cycles as load is increased.

Chapter 5: Conclusion, recommendations, and future work

5.1 Conclusion

In this study, analysis of crack initiation and investigations of the fatigue life of a cracked wheel were carried out through isolation of the regions of maximum von Mises stress at the wheel/rail contact as the most critical crack-initiation zones, then integrated ANSYS-derived stress data with FRANC3D's Paris-law fatigue model to predict life cycles under both rated and overload conditions.

The following conclusions can be drawn from this study.

- The FE-simulations reveal that under rated loading the peak surface stress is 578 MPa, rising to 635 MPa under overload, and that crack orientation in the rolling direction further amplifies stress to 1,225 MPa (rated) and 1,347 MPa (overload).
- The isolated regions were analyzed by a developed approach that combined use of coded databases (cdb) from ANSYS and damage equations in FRANC3D to not only obtain the stress distributions under rated or overload conditions, but also with a small crack oriented in the longitudinal (direction of motion), lateral, and vertical sense.
- Fatigue-life cycles calculated via Paris' law correlate directly with the Stress Intensity Factor range (ΔK), and the fatigue simulations showed that material constants C and m dictate life predictions.
- The fatigue analysis also demonstrated that longer initial cracks drastically reduce life cycles as K_{IC} is approached. This further showed the sensitivity of fatigue life to crack size.

5.2 Recommendations

The obtained results, as discussed above, offer a procedure into determination of the amount of cycles that could cause a relatively small crack to turn critical hence causing further damage to the wheel treads as used in daily service in order to mitigate the risks identified in this research's conclusions.

The following recommendations can be made:

- Given the significant increase in peak surface stress under overload conditions, efforts should be made to operate within the rated loading capacity to extend the lifespan of the wheel tread.
- Timely repair for wheels with detected critically sized cracks to ensure that the damage does not progress rapidly and unstably leading to fatal scenario occurrences.
- Since fatigue life is linked to stress cycles, operational data (like distance traveled and load history) can be used to predict when critical stress thresholds might be reached.

Nonetheless, the following recommendations are suggested for any future studies that may be related to similar work done within this study.

- Analysis on the relationship between speed and stress under both rated and overload conditions to identify optimal speed ranges that minimize peak stresses and fatigue damage.

- An investigative study on the effects of variation of the crack lengths using other models such as NASGRO or Elber Model.

- A study on the influence of the nonlinear behavior as the crack's length nears criticality to the variation of the Stress Intensity Factors.

- A FEA and approach that takes into account the effects of temperature and any other operational condition subject to LRT.

- Experimental determination of the critical Stress Intensity Factors for LRT wheels using AALRT as the case study.

References

[1] D. Baranovskyi, L. Muradian, and M. Bulakh, "The Method of Assessing Traffic Safety in Railway Transport," *IOP Conf. Ser. Earth Environ. Sci.*, vol. 666, no. 4, p. 042075, Mar. 2021, doi: 10.1088/1755-1315/666/4/042075.

[2] V. G. Struchalin, E. Yu. Narusova, I. V. Paruleva, I. S. Procopchuk, and A. S. Lebedeva, "Development of Robotic Systems to Improve the Safety of Railway Transport Operations," in *2022 Conference of Russian Young Researchers in Electrical and Electronic Engineering (ElConRus)*, Jan. 2022, pp. 1749–1752. doi: 10.1109/ElConRus54750.2022.9755479.

[3] S. Wieczorek, K. Pałka, and B. Grabowska-Bujna, "A MODEL OF STRATEGIC SAFETY MANAGEMENT IN RAILWAY TRANSPORT BASED ON JASTRZEBSKA RAILWAY COMPANY LTD.," *Sci. J. Silesian Univ. Technol. Ser. Transp.*, vol. 98, pp. 201–210, Mar. 2018, doi: 10.20858/sjsutst.2018.98.19.

[4] H. Ishida and M. Matsuo, "Safety Criteria for Evaluation of Railway Vehicle Derailment," *Q. Rep. RTRI*, vol. 40, no. 1, pp. 18–25, 1999, doi: 10.2219/rtriqr.40.18.

[5] U. M. Cherkashin, S. M. Zakharov, and A. E. Semechkin, "An overview of rolling stock and track monitoring systems and guidelines to provide safety of heavy and long train operation in the Russian Railways," *Proc. Inst. Mech. Eng. Part F J. Rail Rapid Transit*, vol. 223, no. 2, pp. 199–208, Mar. 2009, doi: 10.1243/09544097JRRT226.

[6] P. Kundu, A. K. Darpe, S. P. Singh, and K. Gupta, "A Review on Condition Monitoring Technologies for Railway Rolling Stock," 2018.

[7] S. Chrismer, E. Sherrock, D. Stone, and A. Alvarez-Reyes, "Wheel Failure Investigation Program: Phase 2".

[8] M.-A. Spiroiu and M. Nicolescu, "Failure modes analysis of railway wheel," *MATEC Web Conf.*, vol. 178, p. 06005, 2018, doi: 10.1051/matecconf/201817806005.

[9] K. Lyu *et al.*, "Analysis on the features and potential causes of wheel surface damage for heavy-haul locomotives," *Eng. Fail. Anal.*, vol. 109, p. 104292, Jan. 2020, doi: 10.1016/j.engfailanal.2019.104292.

[10] S. Agrawal and R. L. Himte, "Evaluation of Bending Stress at Fillet Region of an Asymmetric Gear with a Hole as Stress Relieving Feature using a Fea Software Ansys," *Int. J. Comput. Appl.*, vol. 51, no. 8, pp. 28–33, Aug. 2012, doi: 10.5120/8064-1450.

[11] M. Kiani and G. T. Fry, "Fatigue analysis of railway wheel using a multiaxial strain-based critical-plane index," *Fatigue Fract. Eng. Mater. Struct.*, vol. 41, no. 2, pp. 412–424, Feb. 2018, doi: 10.1111/ffe.12697.

[12] B. Jang, S. Singh, A. PRABHAKARAN, T. OMAR, and M. STEWART, "Development of Advanced Railway Wheel Life Model for Rolling Contact Fatigue Crack Initiation including the Effect of Residual Stresses," May 2023.

[13] N. Mandefro, "SIMULATION OF CRACK PROPAGATION OF A SKIDDED RAIL WHEEL USING EXTENDED FINITE ELEMENT METHOD (XFEM)".

[14] R. Wirtu, "Thermo-Mechanical Analysis of Railway Wheel – Rail Rolling/Sliding contact".

[15] M. Freisinger, A. Trausmuth, R. Hahn, and E. Badisch, "Influence of the evolution of near-surface rail wheel microstructure on crack initiation by micro-bending investigations," *Proc. Inst. Mech. Eng. Part F J. Rail Rapid Transit*, vol. 238, no. 2, pp. 249–255, Feb. 2024, doi: 10.1177/09544097231191550.

[16] A. M. G. Langueh, J. -F. Brunel, E. Charkaluk, P. Dufrénoy, J. -B. Tritsch, and F. Demilly, "Effects of sliding on rolling contact fatigue of railway wheels," *Fatigue Fract. Eng. Mater. Struct.*, vol. 36, no. 6, pp. 515–525, Jun. 2013, doi: 10.1111/ffe.12020.

[17] M. Asplund, *Wayside condition monitoring system for railway wheel profiles: applications and performance assessment*. Luleå: Luleå University of Technology, 2016.

[18] M. M. Chatzimichailidou, A. Martinetti, and A. Majumdar, "Wheel maintenance in rolling stock: safety challenges in the defect detection process".

[19] A. Alemi, F. Corman, and G. Lodewijks, "Condition monitoring approaches for the detection of railway wheel defects," *Proc. Inst. Mech. Eng. Part F J. Rail Rapid Transit*, vol. 231, no. 8, pp. 961–981, Sep. 2017, doi: 10.1177/0954409716656218.

[20] A. Heckmann, A. Keck, I. Kaiser, and B. Kurzeck, "The Foundation of the DLR RailwayDynamics Library: the Wheel-Rail-Contact," presented at the the 10th International Modelica Conference, March 10-12, 2014, Lund, Sweden, Mar. 2014, pp. 465–475. doi: 10.3384/ecp14096465.

[21] "The Wheel/Rail-Interface Study," Global Railway Review. Accessed: Oct. 17, 2024. [Online]. Available: https://www.globalrailwayreview.com/article/74556/the-wheel-rail-interface-study/

[22] R. Lewis and U. Olofsson, *Wheel-Rail Interface Handbook*. Elsevier, 2009.

[23] Y. Zhu, W. Wang, R. Lewis, W. Yan, S. R. Lewis, and H. Ding, "A Review on Wear Between Railway Wheels and Rails Under Environmental Conditions," *J. Tribol.*, vol. 141, no. 120801, Sep. 2019, doi: 10.1115/1.4044464.

[24] X.-Y. Fang, W. Huang, X.-F. Yang, and J.-G. Wang, "Effects of temperature on fatigue cracks initiation and propagation for a high-speed railway wheel rim steel," *Eng. Fail. Anal.*, vol. 109, p. 104376, Jan. 2020, doi: 10.1016/j.engfailanal.2020.104376.

[25] L. Zhou, Y. Hu, H. H. Ding, Q. Y. Liu, J. Guo, and W. J. Wang, "Experimental study on the wear and damage of wheel-rail steels under alternating temperature conditions," *Wear*, vol. 477, p. 203829, Jul. 2021, doi: 10.1016/j.wear.2021.203829.

[26] M. Shen, B. Rong, Q. Li, M. Yu, Y. Xiao, and H. Zhao, "Different responses of wheel–rail interface adhesion and wheel surface damage induced by an out–of–round wheel tread," *Wear*, vol. 526–527, p. 204956, Aug. 2023, doi: 10.1016/j.wear.2023.204956.

[27] Yingbin L. I. U., Yanhua G., Qiang W., Wei G. a. O., and Zhefeng Z., "Evaluation of Rolling Contact Fatigue Crack of Train Wheels," *TRIBOLOGY*, vol. 40, no. 3, pp. 305–313, May 2020, doi: 10.16078/j.tribology.2019210.

[28] M. R. K. Vakkalagadda and K. P. Vineesh, "Causes and failure forms of railway wheels," *Mater. Today Proc.*, vol. 98, pp. 97–101, Jan. 2024, doi: 10.1016/j.matpr.2023.09.161.

[29] A. Mazzù, C. Petrogalli, M. Lancini, A. Ghidini, and M. Faccoli, "Effect of Wear on Surface Crack Propagation in Rail–Wheel Wet Contact," *J. Mater. Eng. Perform.*, vol. 27, no. 2, pp. 630–639, Feb. 2018, doi: 10.1007/s11665-018-3185-1.

[30] Y. Zhou, J. Sun, X. Pan, G. Qian, and Y. Hong, "Microstructure evolution and very-high-cycle fatigue crack initiation behavior of a structural steel with two loading intermittence modes," *Int. J. Fatigue*, vol. 161, p. 106904, Aug. 2022, doi: 10.1016/j.ijfatigue.2022.106904.

[31] A. Nazari and P. Hosseini-Tehrani, "Using the fatigue crack initiation parameter for prediction of the crack location on a curved track by 3D-FE analysis," *Proc. Inst. Mech. Eng.*

Part F J. Rail Rapid Transit, p. 09544097231203269, Sep. 2023, doi: 10.1177/09544097231203269.

[32] "Microstructural characterization of ... | Open Research Europe." Accessed: Mar. 27, 2024. [Online]. Available: https://open-research-europe.ec.europa.eu/articles/3-73/v2

[33] M. Maglio *et al.*, "Railway wheel tread damage and axle bending stress – Instrumented wheelset measurements and numerical simulations," *Int. J. Rail Transp.*, vol. 10, no. 3, pp. 275–297, May 2022, doi: 10.1080/23248378.2021.1932621.

[34] T. Tang, J. Peng, J. Li, Y. Wan, X. Liu, and R. Ma, "Wheel Tread Reconstruction Based on Improved Stoilov Algorithm," *Optics*, vol. 3, no. 2, Art. no. 2, Jun. 2022, doi: 10.3390/opt3020016.

[35] M. Maglio, T. Vernersson, J. C. O. Nielsen, A. Ekberg, and E. Kabo, "Influence of railway wheel tread damage on wheel–rail impact loads and the durability of wheelsets," *Railw. Eng. Sci.*, vol. 32, no. 1, pp. 20–35, Mar. 2024, doi: 10.1007/s40534-023-00316-2.

[36] S. Li, Q. Xiao, W. Yang, C. Yang, and Y. Wang, "Influence of Axle Weight and Frequency on the Tribological Properties of Laser-Repaired 316L Stainless Steel Coatings in Railway Wheel Tread Braking," *Coatings*, vol. 14, no. 1, Art. no. 1, Jan. 2024, doi: 10.3390/coatings14010113.

[37] S. Zhang *et al.*, "Gaps, challenges and possible solution for prediction of wheel–rail rolling contact fatigue crack initiation," *Railw. Eng. Sci.*, vol. 31, no. 3, pp. 207–232, Sep. 2023, doi: 10.1007/s40534-023-00302-8.

[38] P. A. Wawrzynek, B. J. Carter, C.-Y. Hwang, and A. R. Ingraffea, "Advances in Simulation of Arbitrary 3D Crack Growth using FRANC3Dv5," *J. Comput. Struct. Eng. Inst. Korea*, vol. 23, no. 6, pp. 607–613, 2010.

[39] A. Jaifu, S. Raeon, and M. Pimsarn, "Study of fatigue crack initiation location of wheel and rail under rolling contact using finite element method," *MATEC Web Conf.*, vol. 192, p. 02012, 2018, doi: 10.1051/matecconf/201819202012.

[40] A. Getnet, "Investigation on the Contact Fatigue of Railway Wheel Using a Critical Plane Model".

[41] "Figure 1 Required friction coefficient values in the wheel-rail contact," ResearchGate. Accessed: Dec. 18, 2024. [Online]. Available: https://www.researchgate.net/figure/Required-friction-coefficient-values-in-the-wheel-rail-contact_fig1_346523746

[42] M.-H. Chien, Y.-E. Wu, K.-L. Liao, and W.-H. Chieng, "Rail profile synthesis with special reference to G_1 continuity," *Proc. Inst. Mech. Eng. Part F J. Rail Rapid Transit*, p. 0954409715621436, Jan. 2016, doi: 10.1177/0954409715621436.

[43] "Workbench User's Guide".

[44] Faculty of Mechanical and Industrial Engineering, Aksum University, Aksum, Ethiopia, A. Gebretsadkan Brhane, S. Tesfaye Mekonone, and Institute of Technology, University of Gondar, Ethiopia, "Numeric simulation of steel twin disc system under rolling-sliding contact," *Tribol. Mater.*, vol. 2, no. 4, pp. 181–188, 2023, doi: 10.46793/tribomat.2023.019.

[45] J. C. Garcia-Prada, C. Castejon, H. Rubio, and A. Bustos, "Methodology to characterize the von Misses stress in the contact between wheel and rail (Test-Rig)," in *2016 18th International Wheelset Congress (IWC)*, Chengdu, China: IEEE, Nov. 2016, pp. 34–38. doi: 10.1109/IWC.2016.8068363.

[46] R. Masoudi Nejad and F. Berto, "Fatigue fracture and fatigue life assessment of railway wheel using non-linear model for fatigue crack growth," *Int. J. Fatigue*, vol. 153, p. 106516, Dec. 2021, doi: 10.1016/j.ijfatigue.2021.106516.

Appendix

Table 10: *Wheel and rail details (reference: AALRT)*

	Detail	Dimensions (mm)
Wheel	Diameter	660
	Flange thickness	21.21
	Flange height	28
Rail	Head width	70
	Tread width	48
	Railhead width	49.4
	Web thickness	15
	Rail base thickness	28
	Base width	125
	Rail height	152

A1: Procedure for analysis

The procedure includes majorly transfer of files into ANSYS using engineering data in Figure 49 and Figure 50, adding the necessary planes using ANSYS SpaceClaim, running static analyses, sub-modeling, and adding necessary commands for obtaining coded databases (.cdb) for both the global model (G_M) and sub-model (S_M).

Properties of Outline Row 4: Wheel

	A	B	C	D	E
1	Property	Value	Unit		
2	Material Field Variables	Table			
3	Density	7800	kg m^-3		
4	Isotropic Secant Coefficient of Thermal Expansion				
5	Coefficient of Thermal Expansion	1.2E-05	C^-1		
6	Isotropic Elasticity				
7	Derive from	Young's Modulus and Po...			
8	Young's Modulus	2.1E+11	Pa		
9	Poisson's Ratio	0.3			
10	Bulk Modulus	1.75E+11	Pa		
11	Shear Modulus	8.0769E+10	Pa		
12	Strain-Life Parameters				
13	Display Curve Type	Strain-Life			
14	Strength Coefficient	9.2E+08	Pa		
15	Strength Exponent	-0.106			
16	Ductility Coefficient	0.213			
17	Ductility Exponent	-0.47			
18	Cyclic Strength Coefficient	1E+09	Pa		
19	Cyclic Strain Hardening Exponent	0.2			
20	S-N Curve	Tabular			
21	Interpolation	Log-Log			
22	Scale	1			
23	Offset	0	Pa		
24	Tensile Yield Strength	5.47E+08	Pa		
25	Compressive Yield Strength	5.47E+08	Pa		
26	Tensile Ultimate Strength	8.79E+08	Pa		
27	Compressive Ultimate Strength	0	Pa		

Figure 49: *Engineering data for the wheel*

Properties of Outline Row 3: Rail

	A	B	C	D	E
1	Property	Value	Unit		
2	Material Field Variables	Table			
3	Density	7800	kg m^-3		
4	Isotropic Secant Coefficient of Thermal Expansion				
5	Coefficient of Thermal Expansion	1.2E-05	C^-1		
6	Isotropic Elasticity				
7	Derive from	Young's Modulus and Po...			
8	Young's Modulus	2.07E+11	Pa		
9	Poisson's Ratio	0.3			
10	Bulk Modulus	1.725E+11	Pa		
11	Shear Modulus	7.9615E+10	Pa		
12	Strain-Life Parameters				
13	Display Curve Type	Strain-Life			
14	Strength Coefficient	9.2E+08	Pa		
15	Strength Exponent	-0.106			
16	Ductility Coefficient	0.213			
17	Ductility Exponent	-0.47			
18	Cyclic Strength Coefficient	1E+09	Pa		
19	Cyclic Strain Hardening Exponent	0.2			
20	S-N Curve	Tabular			
21	Interpolation	Log-Log			
22	Scale	1			
23	Offset	0	Pa		
24	Tensile Yield Strength	6.4E+08	Pa		
25	Compressive Yield Strength	6.4E+08	Pa		
26	Tensile Ultimate Strength	8.8E+08	Pa		
27	Compressive Ultimate Strength	0	Pa		

Figure 50: *Engineering data for the rail*

A2: Coded databases (.cdb) extraction

Global model (G_M.cdb)

Load ANSYS Workbench → importing *.STEP* file (Wheel/rail model) → Material assignment →Meshing → Named Selections (cut boundaries) → adding boundary conditions (vertical loads, displacements, and fixed supports) → Commands (for G_M) → Solution

Sub-model (S_M.cdb)

Sub-branch in ANSYS Workbench environment → importing .STEP file (wheel/rail model) → loading model in ANSYS SpaceClaim → adding cutting planes (creating the wheel sub-model/section) → ANSYS Mechanical → Material assignment → Meshing → importing *cut boundary constraints* → Named Selections (including creating nodal components) → Commands (for S_M) → Solution.

Commands

```
1  !   Commands inserted into this file will be executed just prior to the ANSYS SOLVE command.
2  !   These commands may supersede command settings set by Workbench.
3
4  !   Active UNIT system in Workbench when this object was created:  Metric (mm, t, N, s, mV, mA)
5  !   NOTE:  Any data that requires units (such as mass) is assumed to be in the consistent solver unit system.
6  !               See Solving Units in the help system for more information.
7
8
9  CDWRITE,DB,G_M,cdb
10
```

Figure 51: *Command for global model*

Commands

```
1  !   Commands inserted into this file will be executed just prior to the ANSYS SOLVE command.
2  !   These commands may supersede command settings set by Workbench.
3
4  !   Active UNIT system in Workbench when this object was created:  Metric (mm, t, N, s, mV, mA)
5  !   NOTE:  Any data that requires units (such as mass) is assumed to be in the consistent solver unit system.
6  !               See Solving Units in the help system for more information.
7
8
9  CDWRITE,DB,S_M,cdb
10
```

Figure 52: *Command for Sub Model database*

The databases were saved in the root folders of the saved workbench project.

A3: Crack model

Importing .cdb file (S_M.cdb) → Selection of *Boundary conditions* and *Mesh facets* to retain → crack insertion, **Figure 53** (semi-elliptic with a =0.75mm and b=1.5mm) → static analysis (combining the *G_M.cdb* with *S_M.cdb* file) → *K* computations → crack growth (automated through adding *C=1e-09* and *n=2.5*) → saving growth history (*X.fcg*) → checking K history after growth → computation for fatigue life cycles → curve plots.

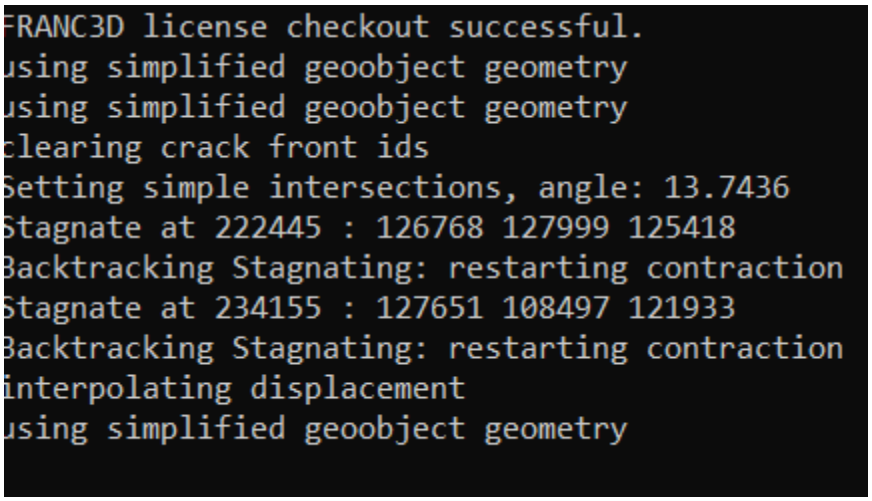

Figure 53: *Crack insertion command prompt window*